Challenge Journal of
CONCRETE RESEARCH LETTERS

Vol.15 No.4 (2024)

acoustic emission aerated concrete artificial neural network compressive strength corrosion cracking ductility durability energy absorption ferrocement flexural strength fly ash fracture mechanics mechanical properties mortar nanoparticle reinforced concrete self- compacting concrete steam curing strengthening superplasticizer tensile strength workability waste disposal water a ption

TULPAR
ACADEMIC PUBLISHING

ISSN 2548-0928

Challenge Journal of Concrete Research Letters

EDITOR-IN-CHIEF

Prof. Dr. Mohamed Abdelkader ISMAIL
Brunel University London, United Kingdom

EDITORIAL BOARD

Prof. Dr. Gamal Elsayed ABDELAZIZ	*Benha University, Egypt*
Prof. Dr. Zubair AHMED	*Mehran University, Pakistan*
Prof. Dr. Ahmet Ferhat BİNGÖL	*Atatürk University, Türkiye*
Prof. Dr. Jiwei CAI	*Henan University, China*
Prof. Dr. Ferit ÇAKIR	*Gebze Technical University, Türkiye*
Prof. Dr. Mohamed GHRICI	*Hassiba Benbouali University of Chlef, Algeria*
Prof. Dr. Khandaker M. Anwar HOSSAIN	*Toronto Metropolitan University, Canada*
Prof. Dr. Jamal KHATIB	*Beirut Arab University, Lebanon*
Prof. Dr. Han Seung LEE	*Hanyang University, Republic of Korea*
Prof. Dr. Jahangir MIRZA	*Hydro-Québec Research Institute, Canada*
Prof. Dr. Ashraf Ragab MOHAMED	*Alexandria University, Egypt*
Prof. Dr. Hamidah Mohd SAMAN	*Universiti Teknologi Mara, Malaysia*
Prof. Dr. Xiao-Yong WANG	*Kangwon National University, Republic of Korea*
Assoc. Prof. Dr. Saleh Omar BAMAGA	*University of Bisha, Saudi Arabia*
Assoc. Prof. Dr. Mohammed Seddik MEDDAH	*Sultan Qaboos University, Oman*
Assoc. Prof. Dr. Brabha NAGARATNAM	*Northumbria University, United Kingdom*
Assoc. Prof. Dr. Ayman Youssef NASSIF	*Vietnamese-German University, Vietnam*

Assoc. Prof. Dr. Meral OLTULU	*Atatürk University, Türkiye*
Dr. Mahmoud SAYED AHMED	*Toronto Metropolitan University, Canada*
Dr. Ibrahim ALAMERI	*Sana'a University, Yemen*
Dr. Salam Rafea ARMOOSH	*University of Anbar, Iraq*
Dr. Aamer Rafique BHUTTA	*Aramco, Saudi Arabia*
Dr. Ali KEYVANFAR	*Kennesaw State University, United States*
Dr. Türkay KOTAN	*Erzurum Technical University, Türkiye*
Dr. Khairunisa MUTHUSAMY	*Universiti Malaysia Pahang, Malaysia*
Dr. Arezou SHAFAGHAT	*Kennesaw State University, United States*
Dr. Jitendra Kumar SINGH	*Hanyang University, Republic of Korea*
Dr. Chunjiang ZOU	*Brunel University London, United Kingdom*

E-mail: *cjcrl@challengejournal.com*

Web page: *cjcrl.challengejournal.com*

Tulpar Academic Publishing
www.tulparpublishing.com

TULPAR ACADEMIC PUBLISHING

Challenge Journal of Concrete Research Letters

CONTENTS

Research Articles

TULPAR
ACADEMIC PUBLISHING

CHALLENGE JOURNAL OF CONCRETE RESEARCH LETTERS 15 (4) (2024) 112–119

Challenge Journal of Concrete Research Letters

Research Article

Determination of waste crushed baked clay aggregate concrete with granular composite material preparations

Fatih Şamdan [a], İbrahim Çelikyürek [b], Mehmet Canbaz [a,*]

[a] *Department of Civil Engineering, Eskişehir Osmangazi University, 26480 Eskişehir, Türkiye*
[b] *Department of Metallurgical and Materials Engineering, Eskişehir Osmangazi University, 26480 Eskişehir, Türkiye*

ABSTRACT

Waste baked clay is an industrial waste that causes environmental pollution. Therefore, the possible utilization of this material would reduce environmental pollution. Utilization of baked clay as aggregate in concrete would have a positive effect on the economy. There are many studies on examining concrete as a granular composite. However, there are few studies on the examination of industrial or construction demolition wastes, which are used as aggregate in concrete, with granular composite models. This study was conducted to contribute to filling this gap in the literature. In concrete production, Portland cement, river sand, 4-32 mm in size crushed stone and crushed baked clay as coarse and medium aggregate in the replacement ratio of 0%, 50% and 100% were used. Compression tests were conducted on specimens. Stress-strain curves were drawn as a graph. Elasticity modulus were determined experimentally. Elasticity modulus were calculated using granular composite models. Experimental and calculated elasticity modulus were compared and examined. According to the results, it was determined that these wastes could be evaluated in concrete production and used in the elasticity modulus calculation of granular composite models.

ARTICLE INFO

Article history:
Received 6 June 2024
Revised 3 July 2024
Accepted 14 July 2024

Keywords:
Waste materials
Baked clay aggregate
Modulus of elasticity
Granular composite models

This is an open access article distributed under the CC BY licence.
© 2024 by the Authors.

1. Introduction

Composite materials are created by combining two or more materials at a macro level to form a new, single material with improved properties. Composite materials are formed by combining matrix and reinforcement materials at an interface. Composite materials reinforced with particles (granular composites) are obtained by distributing the particles homogeneously in a matrix material (Yusuf 2022). Concrete can be given as an example of granular composites. Cement paste is used as matrix material in concrete, and aggregate is used as reinforcement material. The concrete components cannot show sufficient mechanical properties on their own. However, when these materials come together at an interface to form a composite material, the mechanical properties of the concrete improve. Aggregates used as reinforcement materials in concrete production are obtained from natural or artificial stones, ceramics, and organic materials. Examples of artificial aggregates include schists and clays, brick-tile pieces, and blast furnace slag (Ersoy 2001). With the increasing demand for new construction and the reconstruction of buildings to improve living standards, the reserves of natural aggregates have been rapidly depleted (Aboalella and Elmalky 2023; Mohamed et al. 2021). It can be used as aggregate in industrial waste. Studies on the utilization of industrial waste in the construction sector continue increasingly (Şengel et al. 2019, 2022a; Güler 2024). Lightweight concrete is produced by replacing normal-weight aggregate with a lighter aggregate to reduce the structure's weight (Mousa et al. 2018). Sustainable lightweight concrete production is aimed at using artificial aggregates in lightweight concrete production. Artificial aggregates such as crushed baked clay (CBC) reduce concrete density and prevent environmental pollution by using less natural aggregate.

In this study, normal aggregates and waste crushed brick and tile produced from baked clay were used as

* *Corresponding author*. Tel.: +90-222-239-3750 ; E-mail address: mcanbaz@ogu.edu.tr (M. Canbaz)
ISSN: 2548-0928 / DOI: https://doi.org/10.20528/cjcrl.2024.04.001

granular material. CBC can be used as artificial aggregate by crushing to appropriate particle size. Türkiye has a production capacity of 12.8 million m^3 of bricks in 163 factories and 307 million tiles in 36 factories. With the rising volume of waste, rapid environmental pollution poses a significant threat to biodiversity and human health. As a result, there has been an increase in research efforts on waste recycling, both in terms of study and implementation (Çelik et al. 2024; Şengel et al. 2022b; Canbaz et al. 2021). Large amounts of brick and tile waste are generated due to losses incurred during production, construction demolition works, and roof repairs (Zhang et al. 2020). Although these wastes do not contain environmentally harmful chemical waste, they cause environmental and visual pollution due to the large amount of waste and the need for extensive disposal areas (Zhao et al. 2018; Yang et al. 2020). Therefore, recycling and using this waste as raw materials for various industrial products is very important.

Klak et al. (2023) examined the recycling of CBC as fine aggregate in concrete and mortar. They used CBC as fine aggregate in different proportions in concrete production. They also examined compressive strength, splitting tensile strength, workability, dry and wet density, and absorption parameters. They stated that the compressive strength of concrete samples decreased.

Dang and Zhao (2019) produced clay brick concrete by replacing sand with CBC in specific proportions. They stated that the compressive strength of CBC concrete increases as the curing age increases. They concluded that the compressive strength was maximum in samples that did not contain extra water. The waste clay brick could absorb free water from the concrete mixture without additional water, reducing the w/c ratio effect. They stated they encountered a decrease at the same ratio when the elasticity modulus was examined.

Bektaş et al. (2009) produced recycled mortar by replacing sand with CBC. They stated that the compressive strength of the mortar produced with fine CBC increased with the curing age due to the pozzolanic effect. They found no significant difference between the compressive strength of the control mortar and the mortar prepared with fine clay.

Aliabdo et al. (2014) produced recycled mortar and concrete in various sizes using CBC. They stated that when CBC was used in certain proportions instead of cement, the compressive strength of the mortar decreased, and when it was used as an additive to cement, a slight increase in the compressive strength was observed. They found that the elasticity modulus decreased as the amount of CBC used increased.

In many studies, CBC has been used as a fine aggregate in different proportions, and many studies have been carried out on compressive strength. Depending on the usage ratios in the studies, a slight decrease in compressive strength and elasticity modulus was observed (Ge et al. 2015; Vieira et al. 2016; Dang and Zhao 2019; Olofinnade and Ogara 2021; Helmy et al. 2023).

This study aimed to produce concrete using CBC aggregates. First, an experimental study was carried out on the stress, strain, and elasticity modulus of the CBC concrete. Then, its mathematical application was made using different rheological models of granular composite materials. For this purpose, parallel phase model - Voigt model, series phase model - Reuss model, combined models, Hirsch-Dougill model, Popovics model, Illston model, Mehmel-Kern model, Bache and Nepper-Christensen model relations and elasticity modulus were found and compared.

The basic models of granular composites are parallel and series phase models that consider properties and volume ratios. Voigt's model called the parallel phase model, consists of parallel connected spring bodies. It predicts that both phases undergo elastic deformation similarly under tension (Voigt 1928). The Reuss model, which is a serial phase model, assumes that the phases that make up the composite will show different deformation under stress occurring in the body depending on the force that creates the composite (Kelly 1990). In the Hirsch-Dougill model, both phases are connected in series in the upper model of the unit element, and a series-connected structure is formed as a whole, with the section consisting of parallel connected phases in the lower part. The obtained formula consists of upper-bound Voigt model and lower-bound Reuss model relations. In the resulting formula, Voigt model values are used as the upper limit, and Reuss model values are used as the lower limit (Dougill 1962; Hirsch 1962). Popovics model consists of series and parallel phase models. In this model, one of the phases forming the composite is considered a serial phase, and the remaining part is considered a completely parallel phase (Popovics and Erdey 1970). The Illston and Mehmel-Kern models are similar. In the Illston model, a horizontal layered approach from the combined models is recommended, and in the Mehmel-Kern model, a vertical layered approach from the combined models is recommended. For both models, it is assumed that there is a square prism at the centre (Manns 1970). Another rheological model is Bache and Nepper-Christensen, which proposes elastic modulus equality depending on phase properties and volume ratios (Bache and Nepper-Christensen 1965).

2. Materials and Method

In concrete production, 4-16 mm and 16-32 mm aggregates were replaced with CBC at 0, 50 and 100%. CBC sizes 4-16 mm are coded "M", and 16-32 mm are coded "C". As seen from Table 1, 300, 350 and 400 cement contents were used in the produced concretes. The amount of water was kept constant at 190 kg/m^3. After one day, the produced samples were removed from the form and stored under standard curing conditions. 28-day compression tests were carried out according to EN 12390-3, and the elasticity modulus was calculated by drawing the stress-strain diagrams of each specimen.

Elasticity modulus was calculated based on the stress and deformations obtained from the compression test applied to the specimen prepared from each component used in production, and the results are given in Table 2.

Table 1. Mixture proportions of concrete.

Mixture, kg		Aggregate (0-4 mm)	Aggregate (4-16 mm - 16-32 mm)	
Cement	Water	Crushed stone	Crushed stone	Baked clay
300		739	581	443
350	190	721	568	434
400		705	555	424

Table 2. Elasticity modulus of ingredients.

	Matrix (binder)	Crushed stone	Baked clay
Elasticity modulus, GPa	7.5	12.27	1.6

Absolute volumes were determined depending on the density of the matrix and granular materials used. Volume ratios were calculated depending on their absolute volume and are in Table 3.

Elasticity modules were calculated mathematically using the elasticity modulus and volume ratios of the composite components in the formulas given in Table 4. Basic models Reuss and Voigt, combined models Hirsch-Dougill, Popovics, IIIston, Mehmel-Kern, and Bache-Nepper-Christensen models were used as calculation methods.

Table 3. Volume ratio of matrix and granular part of composites.

Volume ratio	Matrix	Baked clay	Crushed stone
C 300-0 M 300-0	0.570	0.000	0.430
C 300-50 M 300-50	0.560	0.117	0.323
C 300-100 M 300-100	0.552	0.233	0.215
C 350-0 M 350-0	0.579	0.000	0.421
C 350-50 M 350-50	0.570	0.114	0.316
C 350-100 M 350-100	0.562	0.228	0.210
C 400-0 M 400-0	0.589	0.000	0.411
C 400-50 M 400-50	0.580	0.111	0.309
C 400-100 M 400-100	0.572	0.223	0.206

3. Results and Discussion

The σ-ε diagrams related to the stress-strain of concrete specimens are given in Fig. 1. The use of CBC caused a reduction in compressive strength, as seen in Fig. 1. Compressive strength was decreased with the use of CBC at a cement content of 300-350 and increased at a cement content of 400. The fact that CBC's compressive strength is lower than the compressive strength of limestone-based aggregate caused a decrease in composite strengths. The increase in cement content and the resulting decrease in w/c ratio caused an increase in strength. Although strain values vary depending on the use of CBC, they generally increase. The low deformation stiffness of CBC was effective here.

Elasticity modulus of CBC concrete was found out by σ-ε diagram. Elasticity modulus was found for the concrete series produced by using granular composite material models as seen in Figs. 2–7. Comparison of experimental elasticity modulus and mathematical elasticity modulus are shown in these figures.

Experimental elasticity modulus was decreased with use of CBC and decrease in the amount of CBC used. This decrease ratio was reached 32% with the use of course CBC in 300 cement content concrete. CBC was less brittle material compared to crush stone for this reason strain was higher and also elasticity modulus of concrete was decreased. Experimental results of elasticity models were given closer results in experiments of 300 cement content 50-100 % course CBC concrete of Hirsch-Dougill model as shown in Fig. 2.

When Fig. 3 is examined, the experimental elasticity modules of 350 doses of concrete containing coarse CBC decreased by up to 36% as the coarse CBC content increased. Since they give similar results for this composite group, it is recommended that the parallel phase Voigt model be used for 50% CBC and the Bache-Nepper-Christensen model be used for 100% CBC.

Table 4. Formulas of granular composite models.

Models	Formulas
Paralell (Voigt)	$E_{c\,Voigt} = E_m \,.\, V_m + E_p \,.\, V_p$
Serial (Reuss)	$\frac{1}{E_{c\,Reuss}} = \frac{V_m}{E_m} + \frac{V_p}{E_p}$
Hirsch-Dougill	$\frac{1}{E_{c\,Hirch-Dougill}} = 0{,}5 \,.\, \left(\frac{1}{E_{c\,Voigt}} + \frac{1}{E_{c\,Reuss}}\right)$
Popovics	$E_{c\,Popovics} = 0{,}5 \,.\, (E_{c\,Voigt} + E_{c\,Reuss})$
IIlston	$E_{c\,Illston} = \left[\frac{1 - \sqrt[3]{V_p}}{E_m} + \frac{\sqrt[3]{V_p}}{E_p \,.\, \sqrt[3]{V_p}^{\,2} + E_m \,.\, (1 - \sqrt[3]{V_p}^{\,2})}\right]^{-1}$
Mehmel-Kern	$E_{c\,Mehmel-Kern} = \frac{\sqrt[3]{V_p}^{\,2}}{\frac{\sqrt[3]{V_p}}{E_p} + \frac{1 - \sqrt[3]{V_p}}{E_m}} + E_m \,.\, \left(1 - \sqrt[3]{V_p^{\,2}}\right)$
Bache ve Nepper-Christensen	$E_{c\,Bache-Nepper-Christensen} = E_p^{\,V_p} \,.\, E_m^{\,V_m}$

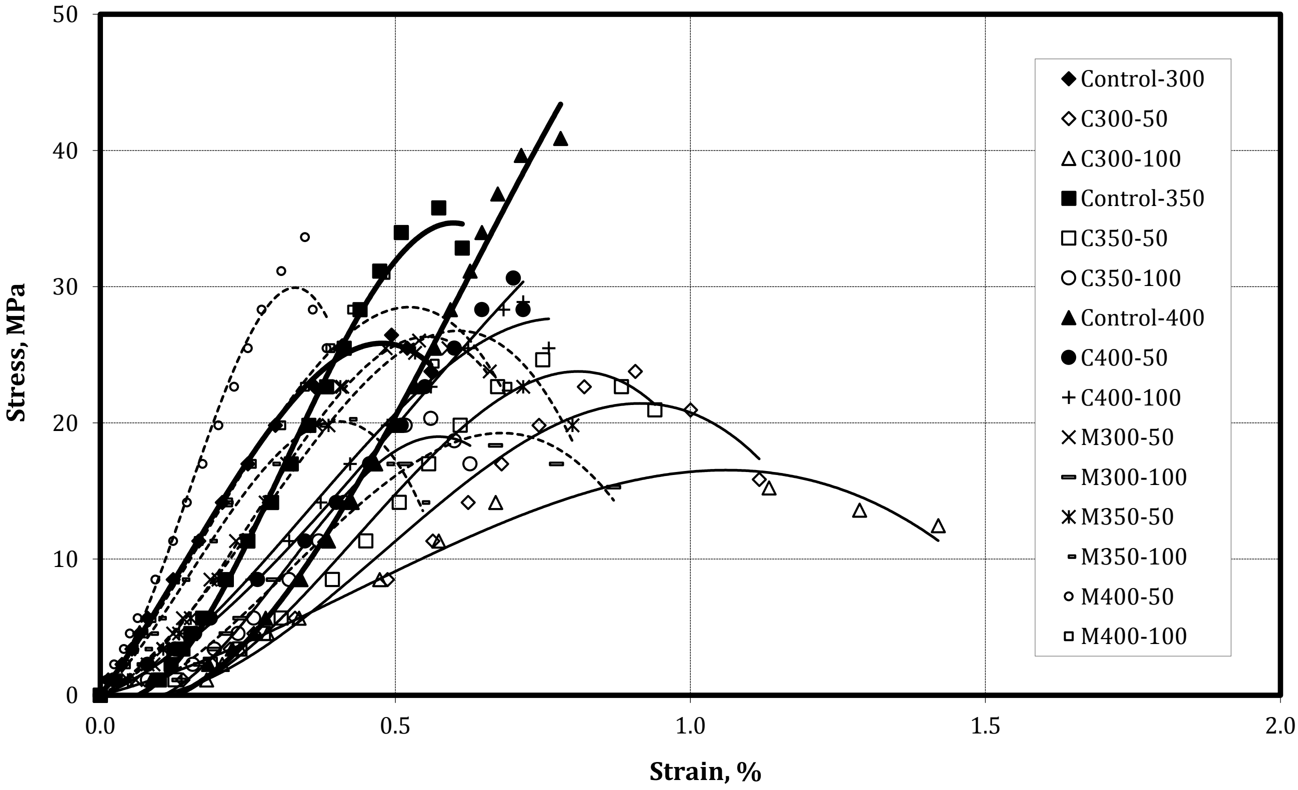

Fig. 1. σ–ε graphs of concrete containing baked clay.

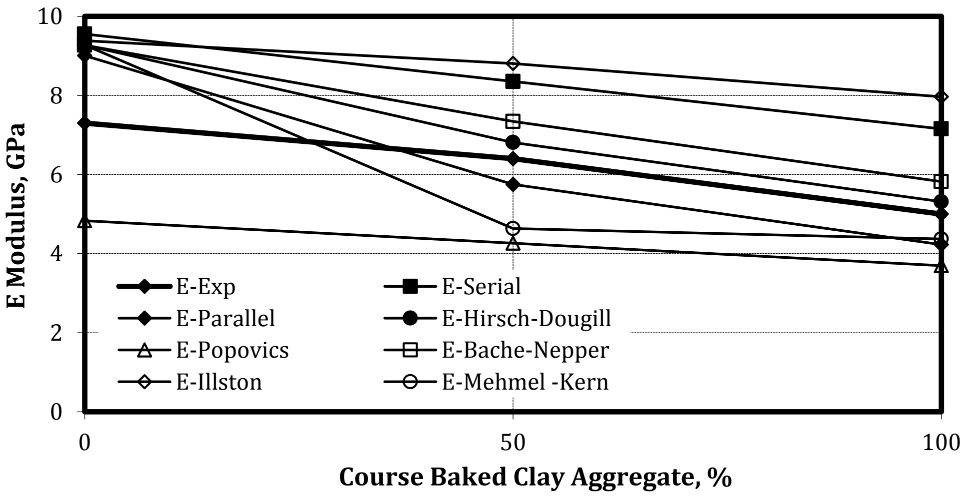

Fig. 2. Elasticity modulus of 300 cement content concrete containing course baked clay aggregate.

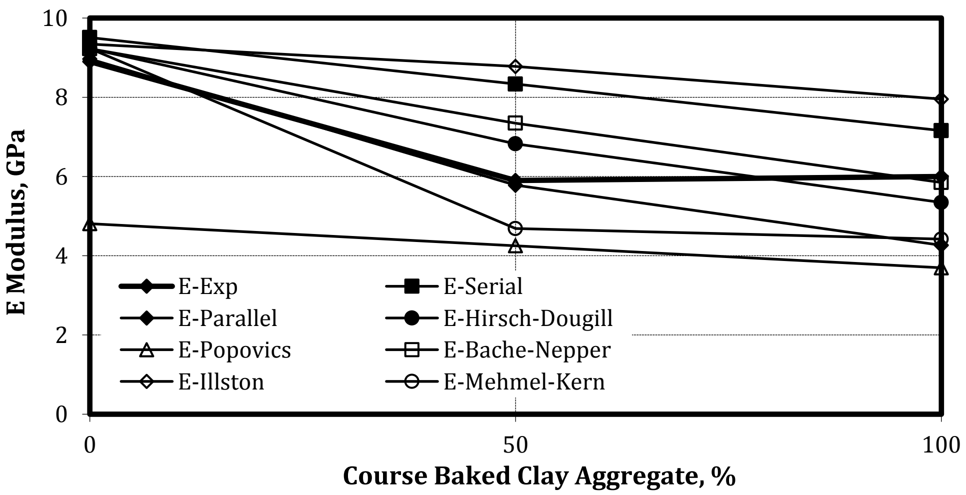

Fig. 3. Elasticity modulus of 350 cement content concrete containing course baked clay aggregate.

In Fig. 4, the experimental elastic modulus of 400 cement content concrete samples containing coarse CBC decreased by up to 29% as the coarse CBC content increased.

The study recommends using the Bache-Nepper-Christensen model for 50% CBC and the parallel phase Voigt model for 100% CBC as they provide similar results for this composite group.

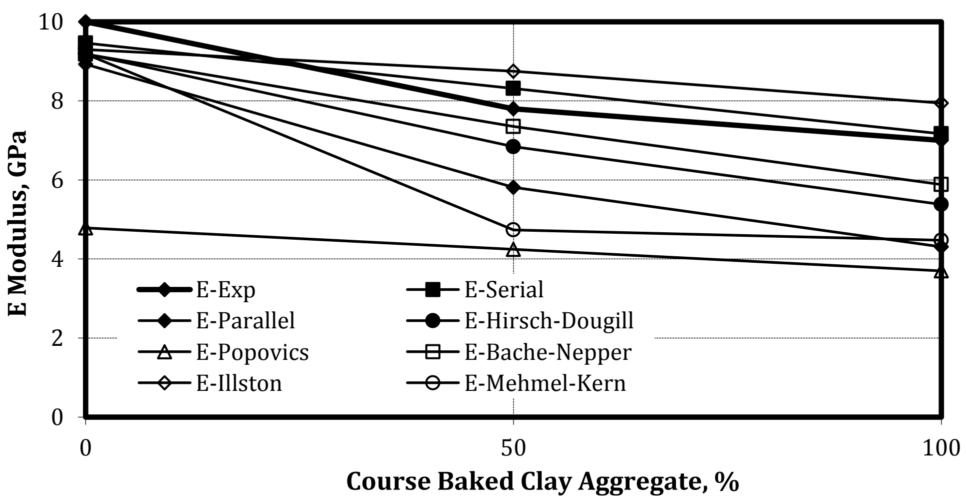

Fig. 4. Elasticity modulus of 400 cement content concrete containing course baked clay aggregate.

In Fig. 5, it was observed that the experimental elastic modulus of 300 concrete samples containing medium CBC decreased by up to 66% as the medium CBC content increased. The study suggests that the Popovics model for 50% and 100% CBC has similar results for this composite group.

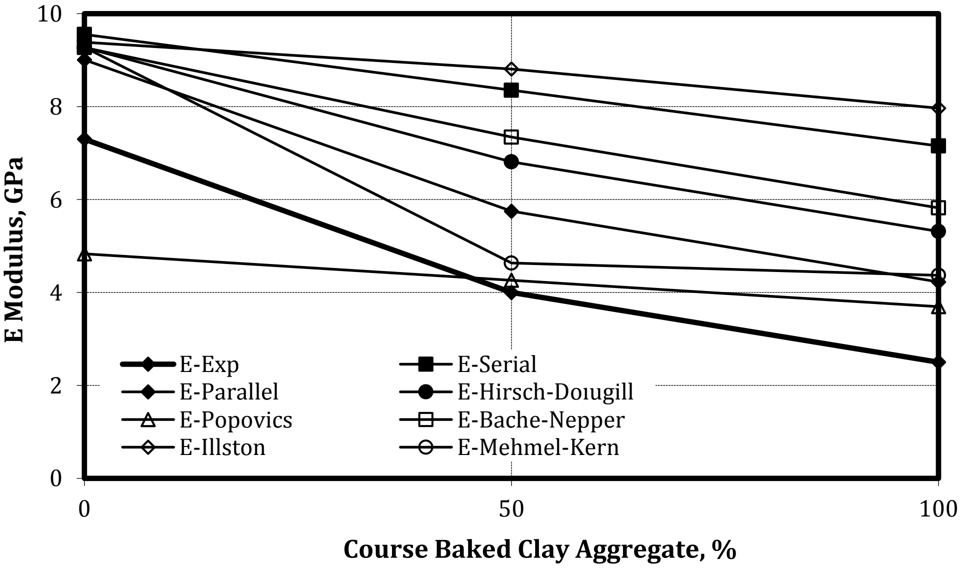

Fig. 5. Elasticity modulus of 300 cement content concrete containing medium baked clay aggregate.

In Fig. 6, the experimental elastic modulus of 350 concrete samples containing medium CBC decreased by up to 42% as the medium CBC content increased. The study recommends using the parallel phase Voigt model for 50% CBC and the Hirsch-Dougill model for 100% CBC as they provide similar results for this composite group.

When Fig. 7 is examined, the experimental elasticity modules of 400 doses of concrete containing medium CBC decreased by up to 36% as the medium CBC content increased. Since they give similar results for this composite group, it is recommended that the parallel phase Voigt model be used for 50% CBC and the Hirsch-Dougill model be used for 100% CBC.

The pointwise closest models of the experimental data obtained using different cement contents and CBC aggregate ratios are stated above. However, as a generalization, the parallel phase Voigt model is more suitable for 50% CBC use, and the Hirsch-Dougill model is more suitable for 100% CBC use. When CBC is coarse, the Hirsch-Dougill model would be more appropriate at low cement contents and the serial-phase Reuss model at high cement contents. When medium CBC is used, the Popovics model is more suitable for low doses, and the Hirsch-Dougill model is more suitable for high cement contents.

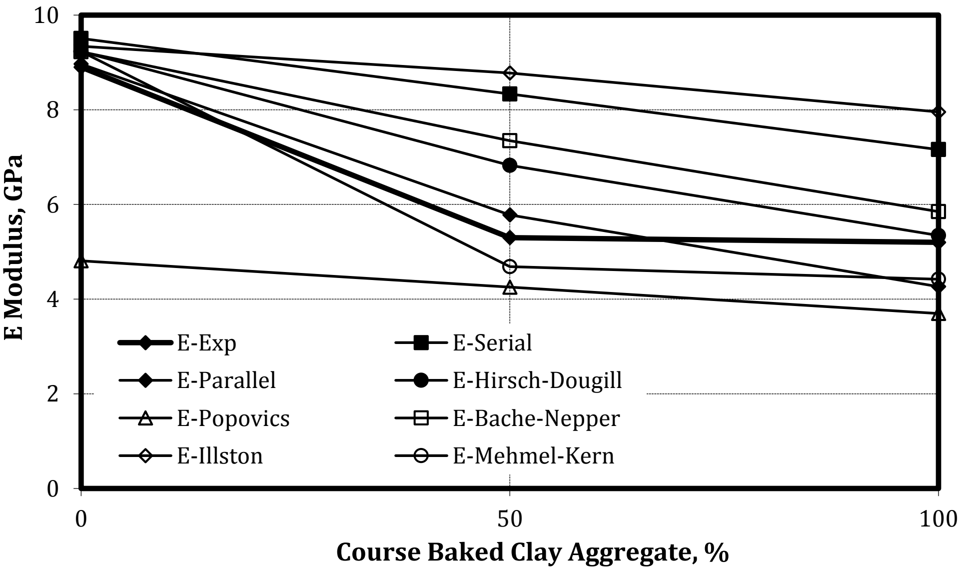

Fig. 6. Elasticity modulus of 350 cement content concrete containing medium baked clay aggregate.

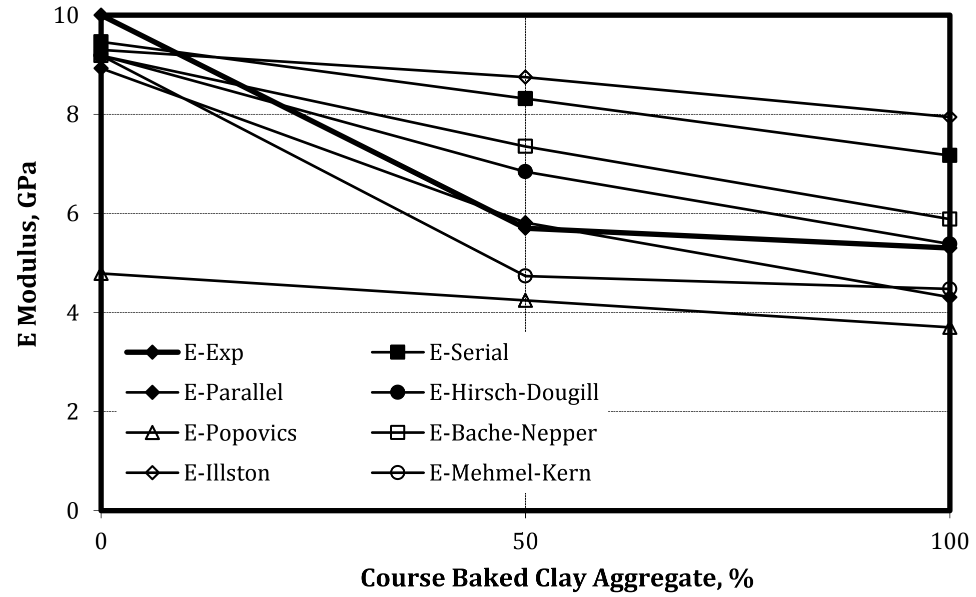

Fig. 7. Elasticity modulus of 400 cement content concrete containing medium baked clay aggregate.

4. Conclusions

The conclusions of the study are summarized as follows:

- As can be seen from the σ–ε graphs obtained from the compression test, while the compressive strength increased with the increase in cement content, it decreased as the use of CBC increased. It has been observed that CBC grains are very important in compressive strength. The use of 100% CBC is not recommended.
- In the specimens where CBC was used, the strength decreased, the deformation increased, and the elasticity modulus decreased compared to the control specimens. By increasing the cement content, the resistance of the binder matrix against deformation increases; thus, an increase in the elasticity modulus is observed.
- The pointwise closest models of the experimental data obtained using different cement contents and CBC aggregate ratios are stated above. However, as a generalization, the parallel phase Voigt model is more suitable for 50% CBC use, and the Hirsch-Dougill model is more suitable for 100% CBC use.
- When CBC is coarse, the Hirsch-Dougill model would be more appropriate at low cement contents and the serial-phase Reuss model at high cement contents. When medium CBC is used, the Popovics model is more suitable for low doses, and the Hirsch-Dougill model is more suitable for high cement contents.

The assessment of waste is crucial for sustainable environmental management. This study shows that the CBC waste generated during production, construction demolition works, and roof repairs can be used in concrete production. However, due to the negative effects of these wastes on mechanical properties, it is recommended to use them in non-load-bearing concrete. In addition, its potential to be used in load-bearing concretes by reducing its negative effects on mechanical properties by using lower ratios can be recommended for new research. It has been demonstrated in this study that granular composite models can also be suitable for concrete containing such wastes.

Acknowledgements

None declared.

Funding

The authors received no financial support for the research, authorship, and/or publication of this manuscript.

Conflict of Interest

The authors declared no potential conflicts of interest with respect to the research, authorship, and/or publication of this manuscript.

Author Contributions

All of the authors made substantial contributions to conception and design, or acquisition of data, or analysis and interpretation of data; were involved in drafting the manuscript or revising it critically for important intellectual content; and gave final approval of the version to be published.

Data Availability

The datasets created and/or analyzed during the current study are not publicly available, but are available from the corresponding author upon reasonable request.

References

Aboalella A, Elmalky A (2023). Use of crushed bricks and recycled concrete as replacement for fine and coarse aggregates for sustainable concrete production. *Challenge Journal of Concrete Research Letters*, 14(2), 39-46.

Aliabdo AA, Abd-Elmoaty A-EM, Hassan HH (2014). Utilization of crushed clay brick in concrete industry. *Alexandria Engineering Journal*, 53, 151–168.

Bache TJ, Nepper-Christensen P (1965). Observation on strength and fracture in lightweight and ordinary concrete. *Proceedings of and*

International Conference on the Structure of Concrete and Its Behaviour under Load, London.

Bektas F, Wang K, Ceylan H (2009). Effects of crushed clay brick aggregate on mortar durability. *Construction and Building Materials*, 23, 1909–1914.

Canbaz M, Kara İ, Topçu İ (2021). Effect of high temperature on the mechanical behavior of cement-bonded wood composite produced with wood waste. *Challenge Journal of Structural Mechanics*, 7(1), 42-48.

Çelik Z, Turan E, Oltulu M, Öner G (2024). Reinforcement of concrete beams using waste carbon-nanoclay-fiberglass laminate pieces. *Challenge Journal of Concrete Research Letters*, 15(1), 1-6.

Dang J, Zhao J (2019). Influence of waste clay bricks as fine aggregate on the mechanical and microstructural properties of concrete. *Construction and Building Materials*, 228, 116757.

Dougill JW (1962). Discussion of modulus of elasticity of concrete affected by moduli of cement paste matrix and aggregate by Hirsch. *Proceedings of the American Concrete Institute*, 1363–1374.

Ersoy HY (2001) Composite Material. Seckin Publishing, İstanbul.

Ge Z, Wang Y, Sun R, Wu X, Guan Y (2015). Influence of ground waste clay brick on properties of fresh and hardened concrete. *Construction and Building Materials*, 98, 128–136.

Güler E. (2024). The effect of dust sugar filter waste on soil dynamic parameters and liquefaction. *Journal of Material Cycles and Waste Management*, 26, 1855–1873.

Helmy SH, Tahwia AM, Mahdy MG, Elrahman MA (2023). Development and characterization of sustainable concrete incorporating a high volume of industrial waste materials. *Construction and Building Materials*, 365, 130160.

Hirsch TJ (1962). Modulus of elasticity iof concrete affected by elastic moduli of cement paste matrix and aggregate. *Journal Proceedings*, 59, 427–452.

Kelly A (1990). Composite Materials: An Overview. Concise Encyclopedia of Building and Construction Materials. Pergamon Press and the MIT Press, UK.

Klak FS, Saleh H, Tais AS (2023). Recycling of crushed clay bricks as fine aggregate in concrete and cement mortar. *Australian Journal of Structural Engineering*, 24, 67–76.

Manns W (1970). On the influence of the elastic properties of cement stone and aggregate on the elastic properties of mortar and concrete. Westdtsch Verl Köln Oplad.

Mohamed A, Abdullah M, Bassam A, Ibrahim S (2021). Effects of nano cotton stalk and palm leaf ashes on ultrahigh-performance concrete properties incorporating recycled concrete aggregates. *Construction and Building Materials*, 302, 124196.

Mousa A, Mahgoub M, Hussein M (2018). Lightweight concrete in America: presence and challenges. *Sustainable Production and Consumption*, 15, 131–144.

Olofinnade O, Ogara J (2021). Workability, strength, and microstructure of high strength sustainable concrete incorporating recycled clay brick aggregate and calcined clay. *Cleaner Engineering and Technology*, 3, 100123.

Popovics S, Erdey MRA (1970). Estimation of the modulus of elasticity of concrete-like composite materials. *Matériaux et Construction*, 3, 253–260.

Şengel HS, Canbaz M, Güler E (2019). Utilization of ceramic waste in the production of Khorasan mortar. *Challenge Journal of Structural Mechanics*, 5(3), 80-84.

Şengel H, Özgören A, Erol H, Canbaz M (2022a). Mechanical behavior investigation of rubberized concrete barriers in impact load. *Challenge Journal of Concrete Research Letters*, 13(3), 93-100.

Şengel H, Kınık K, Erol H, Canbaz M (2022b). Effect of waste steel tire wired concrete on the mechanical behavior under impact loading. *Challenge Journal of Structural Mechanics*, 8(4), 150-158.

Vieira T, Alves A, De Brito J, Correia JR, Silva RV (2016). Durability-related performance of concrete containing fine recycled aggregates from crushed bricks and sanitary ware. *Materials & Design*, 90, 767–776.

Voigt W (1928). Textbook of Crystal Physics. Leipzig, Germany: B.G. Teubner.

Yang D, Liu M, Ma Z (2020). Properties of the foam concrete containing waste brick powder derived from construction and demolition waste. *Journal of Building Engineering*, 32, 101509.

Yusuf S (2022). Introduction to Composite Materials. Seçkin Publishing, İstanbul.

Zhang S, He P, Niu L (2020). Mechanical properties and permeability of fiber-reinforced concrete with recycled aggregate made from waste clay brick. *Journal of Cleaner Production*, 268, 121690.

Zhao Y, Gao J, Chen F, Liu C, Chen X (2018). Utilization of waste clay bricks as coarse and fine aggregates for the preparation of lightweight aggregate concrete. *Journal of Cleaner Production*, 201, 706–715.

Challenge Journal of Concrete Research Letters

Research Article

Calcium aluminate cement based high early strength engineered cementitious composites with recycled artificial flaws

Ahmed Latif Kadhim [a], Süleyman Bahadır Keskin [a,*]

[a] *Department of Civil Engineering, Muğla Sıtkı Koçman University, 48000 Muğla, Türkiye*

ABSTRACT

Engineered Cementitious Composites (ECC) is an ideal repair material due to its high durability and ductility. However, providing ECC with high early strength is challenging since strength and ductility, which are key to crack-free repair, are also interdependent. Thus, it is necessary to use artificial flaws in order to keep the ductility at reasonable levels while increasing the strength. This study uses calcium aluminate cement, a non-portland cement, as the primary binder to attain the early strength in the production of high early strength ECC for the first time. Besides, expanded glass and crumb rubber, both made by recycling waste materials, were included as artificial flaws to enhance ductility. The performance of designed high early strength ECC was assessed through mechanical, abrasion, shrinkage and non-destructive tests and compared with high early strength portland cement based ECC. It is revealed that a minimum compressive strength of 28.9 MPa and flexural strength of 7.1 MPa could be attained even at the age of as early as 6 hours after casting. Nevertheless, deformation capacities were significantly improved after 24 hours following the casting by the use of both artificial flaws. In addition, acceptable drying shrinkage and abrasion resistance values were obtained.

ARTICLE INFO

Article history:
Received 12 June 2024
Revised 10 July 2024
Accepted 1 August 2024

Keywords:
Engineered cementitious composites
Expanded glass
Crumb rubber
Calcium aluminate cement
White portland cement

This is an open access article distributed under the CC BY licence.
© 2024 by the Authors.

1. Introduction

Concrete structures are susceptible to deterioration due to low durability emerging from insufficient tensile strength and ductility (Frangopol and Furuta 2001). Whether the major cause of damage is an internal or an environmental condition, mechanical loading, or even their combination (FHWA 1998; Yunovich and Thompson 2003) they influence the serviceability of structures and threaten human safety. Repair, retrofit, and maintenance of existing structures emerge as an immediate necessity as failure may occur catastrophically if the structures are left in their current condition. While many well-established techniques have been suggested for retrofitting until now, significant engineering and economic challenges remain (Tarhan and Uysal 2024). Studies addressing this issue show that billions of dollars are spent yearly in the USA (Yunovich and Thompson 2003; Emmons and Sordyl 2006) and Asia, and maintenance and repair expenses account for roughly half of the building budget in the UK (Raupach 2006). The total estimated cost of rehabilitation of infrastructures is enormous, reaching multiple trillion dollars in the US and Asia separately and not less than tens of billion dollars on annual basis with repair costs exceeding the cost of new constructions in Europe and Far Eastern countries (Woudhuysen and Abley 2004; Şahmaran and Li 2010).

Although the need for repair and maintenance is inevitable, the repair materials most of the time are not sufficient to meet this need. It is reported that half of the repair fails prematurely while three-quarters of the failure is due to a deficiency in the durability of the repair material (Whiting and Nagi 1994; Emmons 1996; Wang and Li 2006; Li and Li 2011a; Yildirim et al. 2015). Thus, there is a significant demand for durable repair materials to address the need for long-lasting repairs and decrease the associated economic burden. Engineered Ce-

* *Corresponding author*. Tel.: +90-252-211-5469 ; E-mail address: sbkeskin@mu.edu.tr (S. B. Keskin)
ISSN: 2548-0928 / DOI: https://doi.org/10.20528/cjcrl.2024.04.002

mentitious Composites (ECC), which offers high ductility and durability, emerges as one prominent example of materials that can solve this problem. ECC is a type of high-performance cementitious composite with fiber reinforcement that is highlighted with characteristics of high ductility with a strain hardening behavior under uniaxially applied tensile stresses (Yokota et al. 2008). Although the ingredients of ECC are not remarkably different from ordinary fiber-reinforced concrete, they should have the properties designated by considering the matrix, fiber, and matrix-fiber interface properties imposed by the micromechanical-based design theory (Li 1994; 1997). ECC can reach a strain capacity ranging from 3 to 5% under tension by using 2% of polyvinyl alcohol (PVA) fibers while providing compressive strengths between 30 to 100 MPa (Li et al. 2001; Li 2003). Having a tensile strain capacity reaching up to 500 times that of ordinary concrete, ECC can also perform similarly under flexural loading (Li et al. 1994; Li 1997; Li and Kanda 1998). ECC is demonstrated to be an extremely durable material even in the cracked state (Sahmaran and Li 2009) due to the limited crack width as it performs a steady-state crack propagation rather than a Griffith-type cracking observed in the brittle cementitious composites. This kind of ductile behavior observed in ECC is only possible when the cracking strength of the matrix is lower than the fiber bridging strength and provided that the matrix fracture toughness is low enough (Li 2003; Yang and Li 2007).

Although ideal repair materials should gain adequate strength at the specified age, no formal criterion for minimum compressive strength is defined in the current standards. However, based on the infrastructural requirements, minimum values of flexural or compressive strengths at specific early ages may be recommended by the authorities (Parker and Lee Shoemaker 1991; Kurtz et al. 1997; Wilson et al. 1999). The chemical and physical deterioration of concrete over time is influenced by the presence and movement of harmful substances within the concrete, combined with the cumulative impact of applied loads. The degradation of the structure must be evaluated to determine the most suitable repair approach (Preetha et al. 2023). In some cases, the repair work should be completed and infrastructural facilities need to be put back into service in a short time which is more notable in the case of pavements as the repair process should take 6 to 8 hours during the evening time in order to be able to reopen the road to the traffic in the following morning (Wang and Li 2006; Li and Li 2011b; Şahmaran et al. 2015).

Therefore, strength gaining of the repair materials should be very rapid during the early age. However, such an increase following a rapid reaction may cause a remarkable shrinkage and result in cracking. Conventional ECC is a preferential long-lasting repair material (Lim and Li 1997; Li 2004) as a result of very low cracking potential owing to the high deformation capacity even though it may exhibit considerable autogenous shrinkage due to the high amount of binders and very low w/c ratio used (Keskin et al. 2014). Nonetheless, cracks may also initiate due to various environmental and service conditions (Whiting and Nagi 1994). Accordingly, for sustainable repair and maintenance, the repair material should be resistant to induced tensile stresses and thus should possess sufficient tensile or flexural characteristics to eliminate the mentioned drawbacks. On the other hand, the design of a high early strength ECC (HES-ECC) requires special attention as the early strength rise in ECC accompanies the increase in the fracture toughness which in turn results in insufficient ductility. To overcome this, several studies were undertaken which used a rapid hardening binder for high early strength together with an artificial flaw to decrease the fracture toughness and therefore maintain adequate ductility. One of the studies used rapid hardening Type I and Type III portland cement along with polypropylene and polystyrene particles as artificial flaws and revealed the positive effect of the artificial flaws on ductility (Wang and Li 2006). Polystyrene beads with Type III cement were also used in another study to produce HES-ECC for repair purposes (Li and Li 2011b). Ground slag and CEM I 52.5 R type (high early strength) portland cement were used as binders in a study where the 50% by volume of the quartz sand used as aggregate in ECC was replaced with saturated lightweight perlite aggregate to produce HES-ECC (Yildirim et al. 2015). Significant reductions in the matrix fracture toughness and improvements in tensile strain capacity were observed with the lightweight aggregate replacement (Şahmaran et al. 2015). In a study, the cracking potential of conventional ECC was reduced through lowering the elastic modulus by the use of micronized recycled rubber as a replacement for iron ore tailings aggregates. Matrix fracture toughness was reduced with the increase in the replacement amount and improved the strain capacity accordingly (Huang et al. 2013).

In this study, two different types of cement namely high early strength white portland cement (WPC) CEM I 52.5 R and calcium aluminate cement were used as binders. Calcium aluminate cement (CAC) is a type of non-portland cement with prominent properties of very high early strength and high durability. Hydration characteristics are completely different from ordinary portland cement (OPC) and due to specific compound composition, binary and ternary systems can be formed by using CAC for particular purposes due to the interactions between the compounds of the CAC and other binders. Previously Kim et al. (Kim et al. 2003) used, as an admixture, 5% CAC of the total cementitious material to modify the viscosity of ECC to be used for shotcreting. Similarly, CAC was also used in 3D printable ECC design as an admixture at low amounts, to provide early flowability and manipulate the rate of hardening (Soltan and Li 2018). It is known that in such binary systems created by combining portland cement with a low amount of calcium aluminate cement, the stiffening is quite rapid due to the immediate ettringite formation. However, in this study as the aim is not set to achieve an immediate stiffening but rather to reach a sufficient early strength at 6 hours, calcium aluminate cement is used as a major binder, an alternative to high early strength portland cement, due to its early strength attributes associated with CA hydration which results in a slower setting but rapid hardening as a result of CAH_{10} formation (Kırca 2006). Literature studies regarding the design of high early strength ECC have not reported the use of CAC as a major binder yet.

Although high early strength types of cement similar to the white portland cement employed in this study have previously been used to produce HES-ECC in the literature, this study stands alone as it evaluates the use of CAC and compares it with a portland-type cement in several aspects including durability and mechanical properties.

Nevertheless, in order to maintain ductility, expanded glass beads and crumb rubber particles were used with both of the binders. Several researchers have focused on the use of crumb rubber in ECC production in order to prevent spalling due to the vapor pressure in the case of a fire in the literature. Crumb rubber was also found to be effective in enhancing the elasticity of normal strength ECC while additional precautions such as using nanomaterials are required to compensate for the reduced strength due to rubber usage (Al-Fakih et al. 2021). A lower elastic modulus is also beneficial in the case of ECC usage for repair purposes as it can decrease the cracking potential (Huang et al. 2013). For this reason, crumb rubber was also incorporated in this study as it can improve ductility and limit cracking potential simultaneously. Spherical expanded glass beads were also utilized as an alternative flaw in this study. Although glass has been used to produce lightweight ECC in previous studies (Li 2012), for the first time thermally expanded glass, made out of recycled glass is used for high early strength purposes due to its distinctive characteristics compared to the rubber particles. Compared to previous studies, this study stands out in terms of providing early strength and ductility in many ways, mainly by using calcium aluminate cement as a major binder. In previous studies, CAC was used as an admixture due to its interaction with portland cement. Although waste rubber has been used in the production of ECC due to its elastic properties and expanded glass due to its low density, these two materials have been considered for the first time as an artificial flaw for high early strength. In addition, artificial flaws were also used with high early strength white portland cement to produce HES-ECC with similar early strength to CAC-based HES-ECC and mechanical, non-destructive, and shrinkage properties were compared. In brief, this study aims to evaluate the potential for producing high early-strength ECC by combining the high early-strength properties of calcium aluminate cement with the deformation capacity provided by the recycled artificial flaws.

2. Materials and Method

2.1. Materials and mixture proportions

In the production of HES-ECC mixtures, two types of cement: white portland cement and calcium aluminate cement were used. White portland cement (CEM I 52.5 R type) was selected due to its high early strength. Calcium aluminate cement conforming to EN 14647 (EN 14647 2007) standard on the other hand is a commonly used binder for repair mortars and is chosen as it can reach its ultimate strength within a day. In addition, as conventional ECC mixtures contain a high amount of fly ash in composition per micromechanical-based design theory, it was decided to use as much fly ash as possible, provided that the mixtures reach sufficient early strength. However, this could only be possible in the case of CAC-containing mixtures. Class C fly ash obtained from the Yatağan thermal power plant, was used as a secondary binder. Detailed chemical analysis and physical properties of the binding materials are provided in Table 1.

Table 1. Chemical compositions and physical properties of the binding materials.

Chemical Analysis	CAC (%)	WPC (%)	Fly Ash (%)
SiO2	3.76	21.6	50.04
Al_2O_3	39.48	4.05	22.85
Fe_2O_3	17.23	0.26	8.02
CaO	36.91	65.7	11.21
MgO	0.45	1.3	2.23
SO_3	0.01	3.3	0.78
Na_2O	0.12	0.03	0.27
K_2O	0.14	0.35	2.50
Physical Properties			
Specific Gravity	3.27	3.06	2.28
Blaine fineness (cm^2/g)	3150	4600	2850

Two types of artificial flaws were used in the production of HES-ECCs, crumb rubber from scrap tires and spherical granules of expanded glass from recycling, to compensate for the matrix fracture toughness, which would otherwise increase due to the use of high-strength binders. Both artificial flaws were included in the mixtures at 5% of the total volume. While the specific gravity of the crumb rubber was 1.15, its particle sizes were in the range of 0.42 to 4.75 mm with the majority larger than 2.36 mm. The specific gravity of the expanded glass granules was 0.4 and the particle sizes ranged from 2 to 4 mm. A picture of both artificial flaws is provided in Fig. 1.

Fig. 1. Artificial flaws used.

Although several types of fibers have been used to produce ECC in the literature, PVA fibers stand out due to exceptional mechanical performance and economic advantages. For this reason, 2% of PVA fibers by volume, as adopted by previous studies following the micromechanical-based design theory, were used in all mixtures throughout the experimental study. The PVA fibers have a specific gravity of 1.3, a length of 8 mm, a diameter of 39 µm, and a tensile strength of 1600 MPa, as provided by the manufacturer.

Polycarboxylate ether-based high range water reducing admixture (HRWRA) corresponding to Type F according to ASTM C494 standard (2013), with a specific gravity of 1.1 and 40% solid content was used to enhance the workability of the mixtures. In addition, in the production of HES-ECC, those include white portland cement as the main binder an accelerating admixture (AA) corresponding to Type C according to ASTM C494 standard (2013) was used to reach the target strength. For the mixtures containing calcium aluminate cement, lithium carbonate (LC) salt was used as an accelerator.

2.2. Test specimen preparation and testing

To decide on the mixture proportions given in Table 2, a preliminary study was carried out in which the consistencies of the mixtures along with the compressive and flexural strengths were evaluated. Although fly ash is a latent hydraulic material, in the first group of mixtures where the calcium aluminate cement is the main binder, sufficient strength values could be reached even without eliminating the use of fly ash, although the amount used is lower than the conventional ECC. Nevertheless, the pozzolanic reaction is very limited due to the lack of portlandite as a product of CAC hydration (Ideker et al. 2019), fly ash may help decrease the fractural toughness and contribute to flexural performance. In the second group of mixtures that contain white portland cement, fly ash replacement resulted in strength values lower than expected. Hence, the second group was produced by using WPC alone as a binder. The proportions of all mixtures used in the study are provided in Table 2.

Table 2. HES-ECC mixture proportions.

Ingredient (kg/m^3)	C-CAC	EG-CAC	R-CAC	C-WPC	EG-WPC	R-WPC
Total water	344	327	327	360	342	342
CAC	812	770	770	-	-	-
WPC	-	-	-	1333	1265	1265
Fly ash	464	440	440	-	-	-
Quartz sand	459	436	436	480	455	455
Expanded glass	-	20	-	-	20	-
Crumb rubber	-	-	58	-	-	58
PVA fiber	26	26	26	26	26	26
HRWRA	12.75	12.10	12.10	13.33	12.65	12.65
LC	0.162	0.154	0.154	-	-	-
AA	-	-	-	13.33	12.65	12.65
Water/Binder	0.27	0.27	0.27	0.27	0.27	0.27
Sand/Binder	0.36	0.36	0.36	0.36	0.36	0.36
Fly ash/Cement	0.57	0.57	0.57	-	-	-
LC/CAC (%)	0.02	0.02	0.02	-	-	-
AA/Binder (%)	-	-	-	1	1	1

A 20-liter capacity planetary-type mixer was used to produce six different HES-ECC mixtures. All solid materials, including binders, silica sand, and lithium carbonate (in the case of CAC) were introduced into the mixer. Water was added slowly while mixing the solid materials until the homogenization of the mixture is reached. HRWRA and PVA fibers were introduced to the mixture subsequently following the water and artificial flaws. Finally accelerating admixture was included in the case of the second group of mixtures.

Immediately after mixing, flow diameters were measured using a 60 mm high flow cone with 70 and 100 mm top and bottom diameters, respectively. The cone was placed on a glass plate and mutually perpendicular diameters were measured. Flow values were also measured for fresh HES-ECCs before fiber was added, a flow diameter of 36±1 cm was aimed before the introduction of PVA fibers for all mixtures used in the study. Although it was possible to achieve higher flow values with the use of additional HRWRA, this was avoided to prevent excessive bleeding.

2.2.1. Mechanical testing

The mechanical performances of the produced HES-ECC specimens were evaluated through compressive and flexural tests conducted at 6 hours, 24 hours, 7 days, and 28 days after casting. The specimens, which were left to cure autogenously in closed molds for the first six hours, were taken out of the molds and subjected to testing. Until testing, the specimens to be used in the consecutive test ages were cured in plastic bags at 95±5% RH and 23±2 Cº. Compressive strengths were determined on cubic specimens with dimensions of 50×50×50 mm following the ASTM C109 standard (2020). Flexural strength and midspan deflection capacities were determined under a four-point bending test setup on prismatic specimens with dimensions of 360×75×50 mm located symmetrically on two supports and two loading rollers 304 and 101 mm apart, respectively. The test was carried out at a loading rate of 0.005 mm/sec by using a deformation-controlled electromechanical universal testing machine. Three specimens were used for all mechanical tests at each test age and the results obtained were averaged.

High early-strength materials are typically susceptible to abrasion even at very early ages as they are designed to restore existing infrastructures so that they can be put into service in a short time. Abrasion could take place as a result of several influences and is dependent on factors such as strength, curing, and aggregates used. Abrasion resistance is of greater importance in this particular case, as weak materials such as artificial imperfections can easily increase wear. Thus, abrasion resistances of the developed HES-ECC mixtures were also investigated based on ASTM C944 (2007) standard along with the other mechanical tests. At each test age, one side of cubic specimens with a side length of 150 mm was abraded with rotary cutters under a load of 197 N for 6 minutes, and the depths of wear were measured.

2.2.2. Drying shrinkage measurements

As repair materials should be free of cracks, to foresee the potential risks related to cracking and evaluate the effect of the artificial flaws, drying shrinkages of the developed HES-ECC mixtures were investigated. For this purpose, three 25×25×285 mm bar specimens with gauge studs located at both ends were prepared for each mixture, and length changes of the bars were measured by ASTM C596-18 (2007) standards. The first comparator readings were taken after the initial curing for 6 hours, then the specimens were subjected to drying at 23±2 °C and 50±5% RH until the end of 90 days during which the intermediate readings were taken at 24 hours, 7 days, 14 days, 21 days, 28 days, 56 days. Distribution of the artificial flaws through the cross section of the HES-ECC bars are shown in Fig. 2.

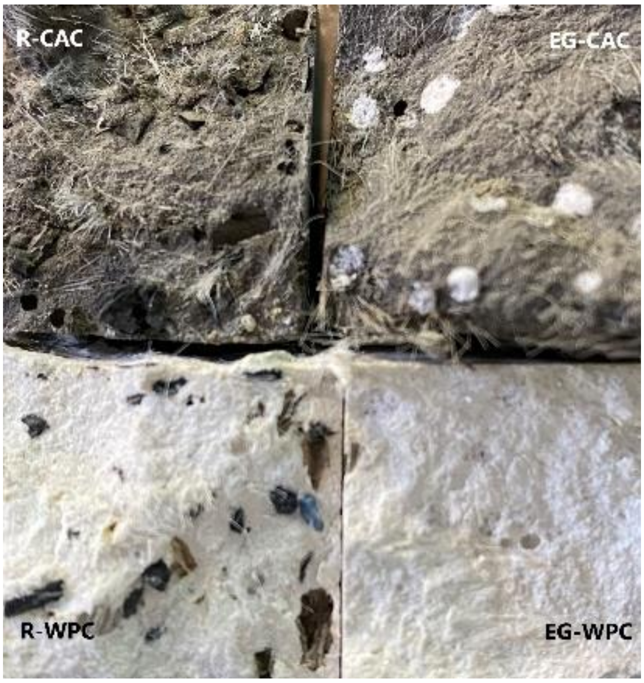

Fig. 2. Distribution of artificial flaws.

2.2.3. Non-destructive testing

Besides the abovementioned tests, non-destructive tests were also conducted on the mixtures to assess the influence of the artificial flaws. Non-destructive methods of ultrasonic pulse velocity (UPV), resonance frequency (RF), and electrical impedance (EI) were applied at the ages of 6 hours, 24 hours, 7 days, and 28 days on beam specimens with the same dimensions employed in bending tests. UPV tests were conducted using an indirect transmission method with transducers capable of generating and receiving 54 kHz ultrasonic waves, located 20 cm apart. RF tests were conducted by measuring the fundamental longitudinal and transverse frequencies of concrete prisms and corresponding dynamic Young's moduli were calculated in accordance with the ASTM C215 standard (1998). The longitudinal frequencies were determined by locating the accelerometer at the center of one end of the specimen and applying the driving force at the opposite end to excite a vibration through the longitudinal axis of the specimen while the transversal frequencies were measured by locating the accelerometer close to the end of one surface and applying the driving force to the middle point of the same surface to excite a transversal vibration. Although the EI is a very fast and practical test, it allows for evaluating the durability and permeability of concrete. During the test, beam specimens were located vertically between the parallel plate electrodes while wet sponges were put between the specimens and the electrodes to provide conductivity. Despite the EI test being a simple yet effective way to evaluate durability, it is based on complicated essence. Due to the polarization effect encountered under direct current, alternating current is used in the test, and impedance is measured which requires to be converted to resistivity later on. Measurements were taken by using alternating current at fixed frequencies of 1 kHz which yields the lowest phase angle of 0^{o} and gives a resistance equal to the impedance. Then, the resistivity of the specimen is calculated by Eq. (1):

$$\rho = \frac{A}{L} z \qquad (1)$$

where ρ, A, L, and Z are respectively the resistivity, cross-sectional area, length, and impedance of the specimen (Spragg et al. 2013).

3. Results and Discussion

3.1. Fresh properties

Flow diameters measured before and after the fiber addition are both provided in Table 3. A matrix slump value of around 36 cm could be achieved by the use of chemical admixtures. In general, although both types of cement have similar matrix consistency, the flow values after the fiber addition were significantly higher for the mixture with WPC. The addition of artificial flaws seems to improve the consistency, as a slightly lower amount of admixtures was needed to achieve the same flow value. In addition, for both types of cement, the flow values of fresh ECC were to some extent higher for the mixtures with flaws.

Table 3. Flow diameters of HES-ECC mixtures with and without fibers.

Mix ID	Matrix (cm)	ECC (cm)
C-CAC	35.5	11.0
EG-CAC	36.0	13.0
R-CAC	36.0	14.0
C-WPC	36.0	16.0
EG-WPC	36.5	18.0
R-WPC	36.0	17.0

3.2. Mechanical performance

Table 4 presents the average compressive strengths for the HES-ECC mixtures at each testing age. For a high early strength repair material, in most cases, the compressive strength at the age of 6 hours is considered as a benchmark. Although the compressive strength to be reached at 6 hours varies according to different sources, in this study a minimum compressive strength of 28.9 MPa even in the presence of flaws could be reached. The control set of CAC mixtures achieved the highest compressive strength at 6 hours due to the rapid formation of calcium alumina hydrates with the help of lithium carbonate salt. The inclusion of the flaws for CAC mixtures resulted in a notable decrease in strength compared to the mixtures with WPC at very early ages. However, as the rate of strength development diminished after 7 days, the gap between the strength of the mixtures was significantly reduced. The control mixture containing WPC, on the other hand, had a lower compressive strength than CAC at 6 hours but eventually surpassed it at later ages. With the use of artificial flaws, a greater reduction in strength was observed in CAC mixtures at early ages, while the decrease in strength of WPC mixtures was more at later ages.

Table 4. Compressive strength of HES-ECC mixtures.

Mix ID	Compressive Strength (MPa)			
	6 hours	24 hours	7 days	28 days
C-CAC	35.2	51.6	57.1	60.6
EG-CAC	29.0	41.2	48.1	56.5
R-CAC	28.9	40.2	44.9	51.8
C-WPC	31.6	52.0	68.9	87.9
EG-WPC	30.2	45.7	58.6	73.3
R-WPC	29.3	41.1	56.6	66.9

The flexural strength and mid-span deflection values of the mixtures as the average of three beam specimens are given in Table 5. Flexural strengths clearly show a similar trend to compressive strengths although the flexural strength development with time was limited since flexural strength is dependent on more complex material characteristics (Qian and Li 2007). Artificial flaws in HES-ECC resulted in a reduction in flexural strength test results across all ages. However, the descending trend was more obvious in the case of incorporating the rubber particles as artificial flaws in R-CAC and R-WPC mixtures which is also evident from the compressive strength results. Even in this case, flexural strength values are well above the values accepted as the minimum flexural strength of concretes to be used for repair purposes by different sources.

Table 5. Flexural behavior of HES-ECC mixtures.

Mix ID	Flexural strength (MPa)				Mid-span beam deflection (mm)			
	6 h	24 h	7 d	28 d	6 h	24 h	7 d	28 d
C-CAC	9.5	9.8	10.9	12.0	6.5	4.2	3.0	3.0
EG-CAC	7.8	9.6	10.7	11.3	4.4	5.5	3.3	3.8
R-CAC	7.3	8.6	10.1	10.8	4.9	5.0	3.8	3.5
C-WPC	7.6	11.9	13.4	13.9	6.8	2.8	2.1	1.9
EG-WPC	7.6	11.5	12.9	13.3	6.4	3.7	3.4	3.9
R-WPC	7.1	10.3	12.2	12.4	7.7	4.3	3.2	3.1

Deformation capacities of the control mixtures began to show a downward trend from the 6th hour due to improved matrix toughness which agrees with Wang and Li (2006) and can be attributed to the development of the interfacial bond between the fibers and the matrix. Despite the decline in deformation capability, deflection hardening tendency is still discernible in Fig. 3 at all ages. The use of artificial flaws yielded conflicting results, especially at the age of 6 hours. This might result from immature matrix fiber and flaw bonding that prevented the early-age HES-ECC mixtures from performing as a complete composite. Still, the rubber appears to perform better compared to expanded glass at this age. However, after 24 hours for both types of artificial flaws, the general trend was to improve the deflection capacity. Although the results did not indicate a predominance of a specific flaw type in improving the deflection value, at the end of 28 days it can be concluded that expanded glass stands out. It should be noted that expanded glass has a brittle nature compared to the ductile and soft rubber particles which have been shown to be effective on the flexural test results (Al-Fakih et al. 2021). It is also noteworthy that although the control mixtures produced with WPC exhibited a drastic decrease in deflection capacity compared to the calcium aluminate cement mixtures, both flaws worked effectively to raise the deflection capacity to a level comparable to the CAC mixtures. Increased deflection values and deflection-hardening behavior of HES-ECC mixtures with artificial flaws may also be attributed to the reduced first crack strength and increased margin for multiple cracking. Sample crack patterns associated with the artificial flaw types is given in Fig. 4.

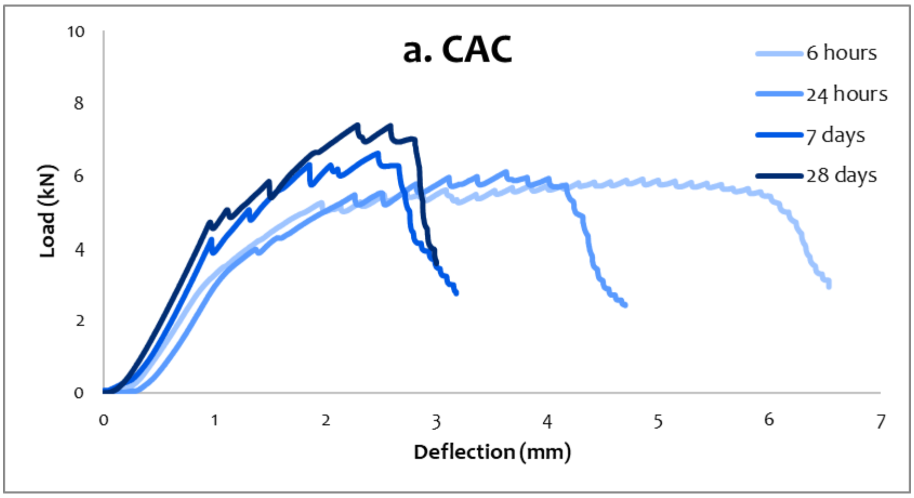

Fig. 3. (continued)

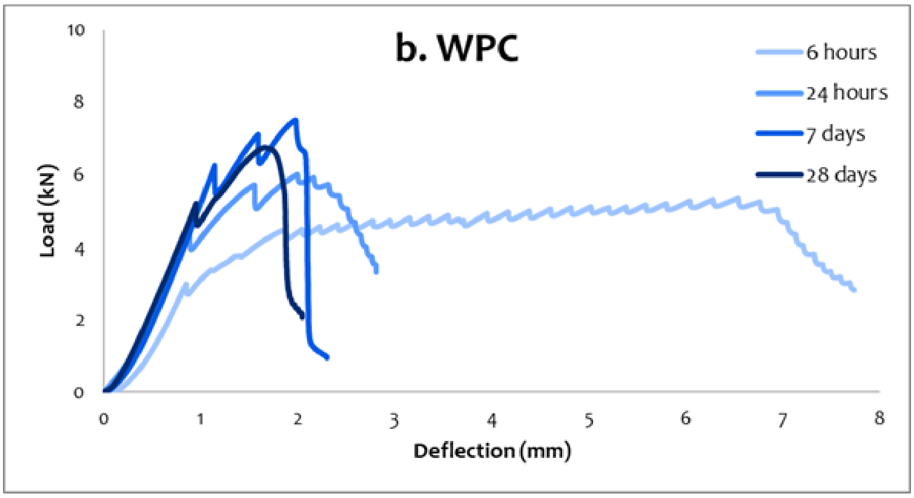

Fig. 3. Comparison of deflections at different ages for the control mixtures.

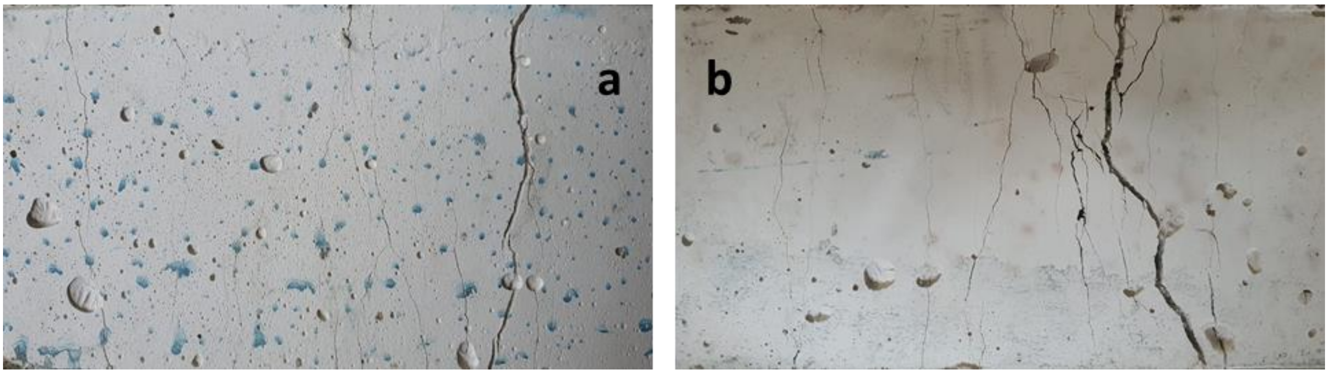

Fig. 4. Multiple cracking of expanded glass (a) and rubber (b) containing beams after failure.

3.3. Abrasion

Abrasion resistance can be a critical property for high early-strength materials and the use of artificial flaws in such materials has the potential to substantially decrease their abrasion resistance. Fig. 5 shows the abrasion depth measured on the diameter of the area worn by rotating cutters for each testing age. It is immediately observable that all CAC and WPC mixtures exhibited an acceptable degree of abrasion resistance at all ages of testing. As the hydration reactions proceeded, the depths of abrasion clearly decreased. Nevertheless, the incorporation of both artificial flaws has a very narrow influence on abrasion resistance. The largest difference which is as low as around 0.05 mm, occurred at the age of 6 hours between the control mixture and the mixture containing rubber as an artificial flaw and may be attributed to pop up of the crumb rubber particles due to immature bond between the rubber and the matrix at this early stage of hydration. Besides, CAC mixtures showed a higher level of abrasion resistance at the early ages, however, the WPC mixtures performed better at the age of 28 days as they reached a higher degree of hydration. Keeping in mind that only 5% of flaws were used in the mixtures, it is difficult to make a comparison between the artificial flaws as the values were quite close but it can be concluded that expanded glass particles yielded a better abrasion resistance.

3.4. Drying shrinkage

For a repair material, lack of dimensional compatibility with the repaired material is of significance as any restraining condition may result in cracking. In most cases, the repair materials are placed on a dimensionally stable existing material which makes the case more threatening. For high-performance materials like ECC, the degree of shrinkage is large due to the high amount of cementitious materials and very low w/c ratio which triggers the chemical shrinkage. Although the cracking resistors such as instantaneous and time-dependent tensile strain capacity of ECC can easily compensate for the shrinkage effect, yet it is important to have an idea of whether the artificial flaws drive the drying shrinkage for the sake of cracking potential. In Fig. 6, the drying shrinkage test results obtained from the length change measurements taken from bar specimens up to 90 days are provided. Drying shrinkage values vary depending on the duration of drying and the presence of artificial flaws in mixtures, as illustrated. The shrinkage values of all calcium aluminate cement mixtures increased remarkably up to 28 days, as expected, while the increase between 28 and 90 days was modest. On the other hand, results indicate that expanded glass and rubber particles have a minor impact on the shrinkage of calcium aluminate cement mixes. After 90 days, the drying shrinkage values for CAC mixtures varied in a short range between 1060 με and 1175 με.

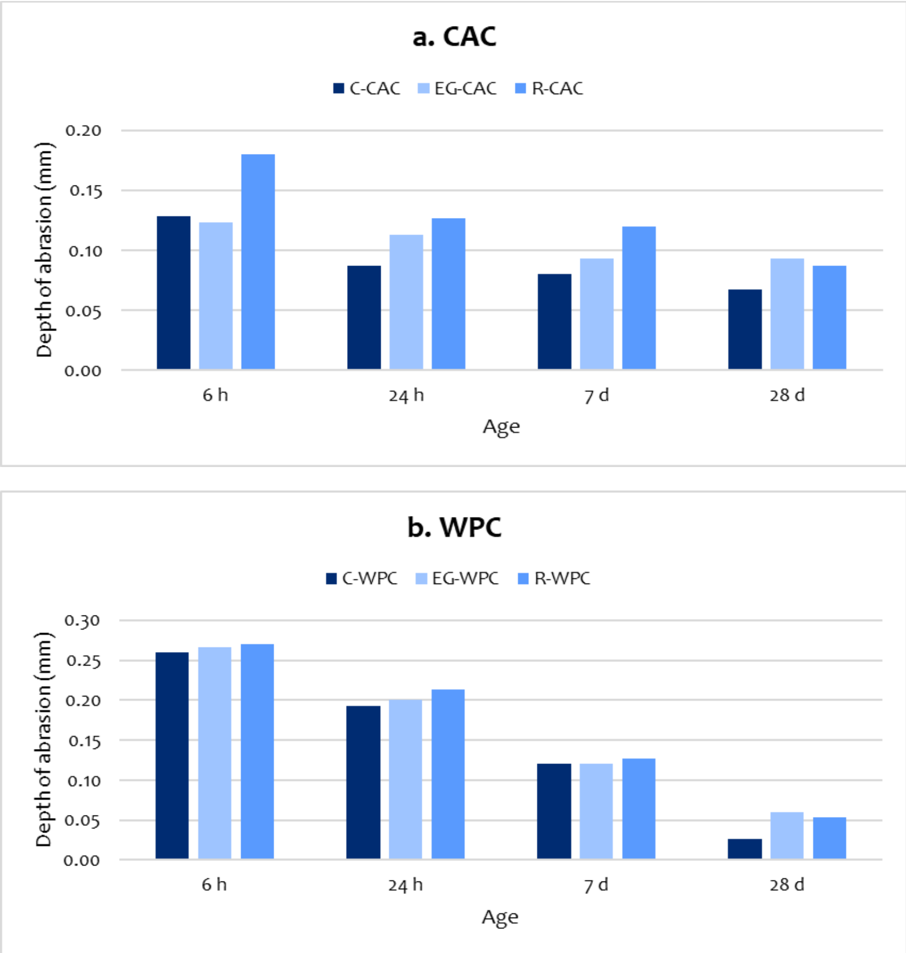

Fig. 5. Abrasion resistance of the mixtures.

Fig. 6 confirms that for all WPC mixtures, drying shrinkage values evolved significantly but not as sharply as for CAC mixtures until 28 days. The influence of artificial flaws on the drying shrinkage of WPC mixtures was more marked. The results revealed that when rubber particles are included in the mix, drying shrinkage rises. Incorporating expanded glass, on the other hand, resulted in the lowest drying shrinkage. The increase in the drying shrinkage in the case of crumb rubber usage as artificial flaws can be ascribed to the decrease of rigid particles to act as a restraint for shrinkage strains in the mixtures as described by Huang et al. (2013). The high absorption capacity of expanded glass may account for the reduction in drying shrinkage for mixtures containing expanded glass, as lightweight aggregates can absorb some of the mixing water and act as reservoirs that release the water during drying as mentioned by Ye et al. (2006) and Keskin et al. (2013).

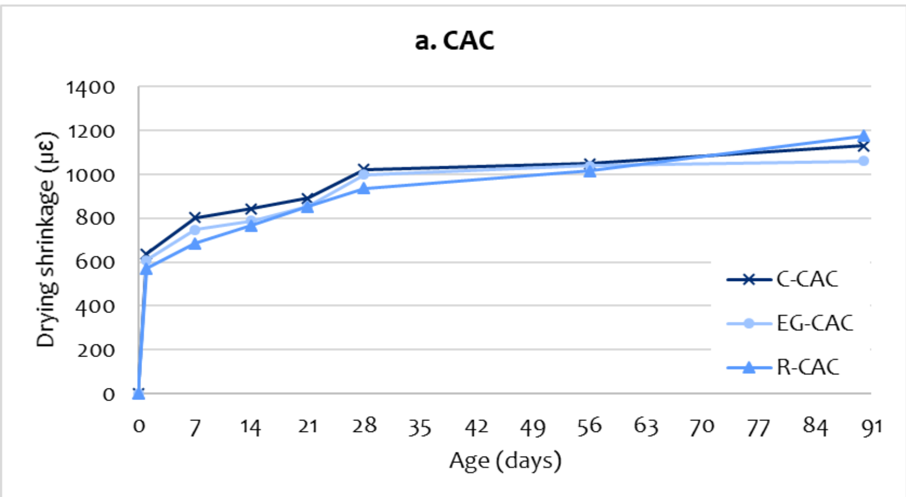

Fig. 6. (continued)

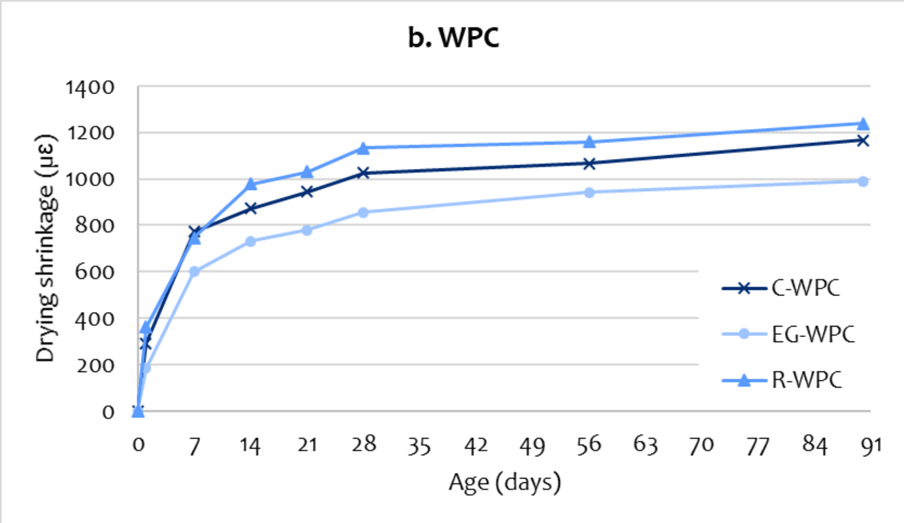

Fig. 6. Drying shrinkage of the mixtures.

3.5. Non-destructive tests

Ultrasonic pulse velocity test was performed conforming to the ASTM C597 (2016) test method by using the indirect transmission method at predetermined testing ages and corresponding pulse velocities were calculated as presented in Table 6. Since UPV values are dependent on the elastic properties of the HES-ECC mixtures, they may serve to evaluate possible changes in the maturity hence the fracture toughness of the ECC mixtures as well. UPV values of all mixtures tested increased with time as hydration reactions progressed. For both of the cement types, the inclusion of artificial flaws resulted in a noticeable decrease in all UPV values, independent of the age of testing.

Nonetheless, UPV values were reduced the most by crumb rubber usage at all ages. This behavior was previously observed by other researchers (Albano et al. 2005; Marie 2016; Choi et al. 2022) as well and attributed to the decrease in the density and increase in the air content due to entrapped air on the rubber surface. Alongside the air entrainment, this reduction may also be ascribed to the damping effect of soft rubber particles.

Table 6. UPV values for HES-ECC prismatic specimens.

Mixture ID	6 hours (m/s)	24 hours (m/s)	7 days (m/s)	28 days (m/s)
C-CAC	4464	4626	4786	4931
EG-CAC	4406	4528	4717	4808
R-CAC	4293	4448	4609	4714
C-WPC	3963	4623	4874	5168
EG-WPC	3945	4508	4818	5072
R-WPC	3924	4369	4763	4992

The resonance frequency is an effective non-destructive test method mainly used for evaluating the concrete properties through the change in the dynamic modulus of elasticity. The test was performed in accordance with the ASTM C215 (1998) method. An accelerometer was employed to obtain the fundamental frequency of vibration for longitudinal and transversal modes after the beam specimen was struck with steel balls. By using the specimen size and mass along with the measured fundamental frequency, the related dynamic modulus of elasticity was calculated. Fig. 7 demonstrates the dynamic elastic modulus values calculated for transverse and longitudinal modes for CAC and WPC containing HES-ECCs. For both longitudinal and transversal modes, the values were close and all mixtures exhibited a similar ascending trend over time. CAC mixtures presented higher elastic modulus at 6 hours however the development of elastic modulus was greater for WPC mixtures. This tendency is also very similar to those observed in compressive and flexural strength test results which is predictable as strength and elastic modulus both increase as the degree of hydration increases. It is obvious that the flaws affect the test results in the same way regardless of the direction of testing. The incorporation of expanded glass contributed to a decrease of an average of 9% in dynamic elastic modulus after 28 days for mixtures with respect to control mixtures due to the weakness of expanded glass and the void content in expanded glass beads. Nevertheless, the lowest values were encountered in mixtures with crumb rubber particles with a decrease of an average of 13% which can be attributed to the high elasticity imparted by the resilient nature of the tire rubber. Moreover, in the case of CAC mixtures, the results obtained with both flaws were closer compared to the WPC mixtures where expanded glass mixtures are quite distinct with a higher elastic modulus which may be due to the bond characteristics of the flaws incorporated.

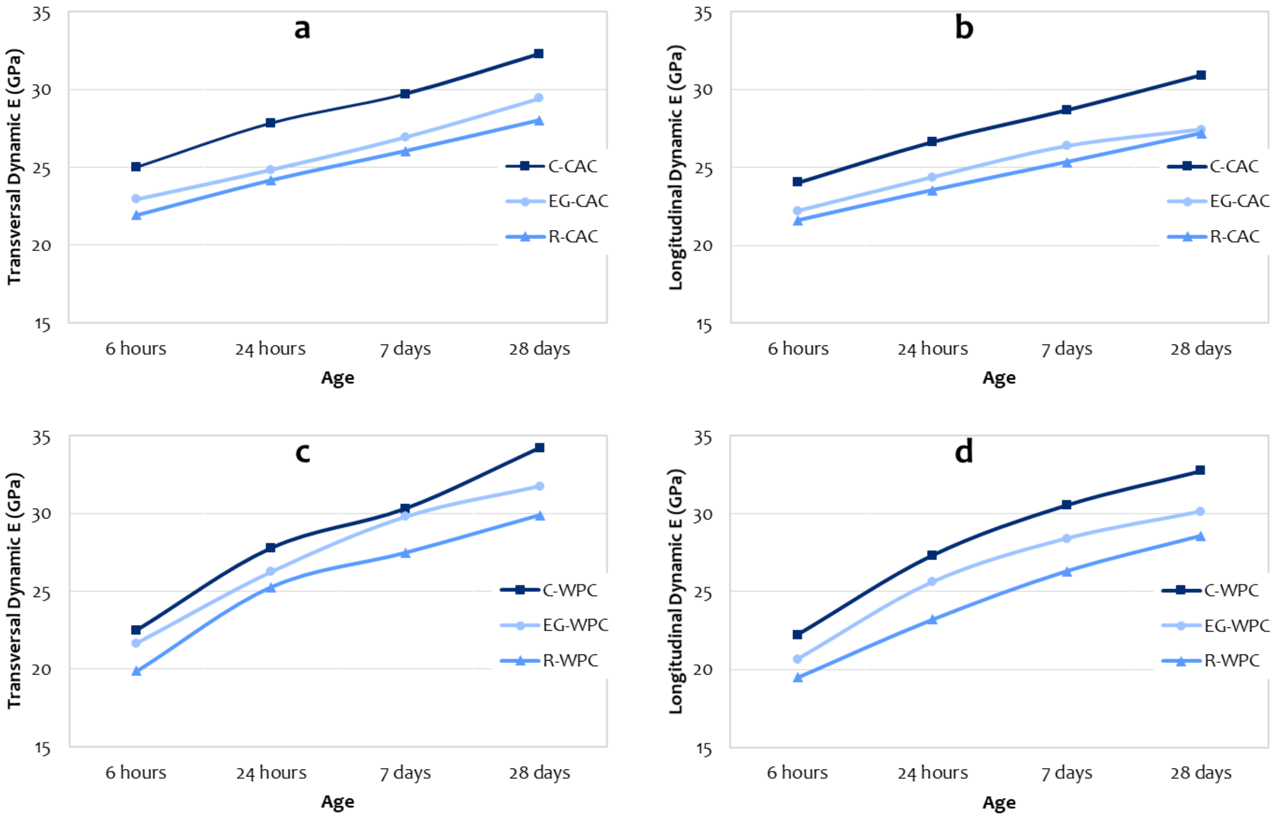

Fig. 7. Transversal (a, c) and longitudinal (b, d) dynamic *E* values for CAC (a, b) and WPC (c, d) mixtures.

The ability of cementitious materials to resist the electrical current is dependent on factors such as permeability, the presence of water in the pores, and the chemistry of the pore solution. As it depends on ion transfer through the specimen, a higher resistivity can infer better durability due to low permeability and a structure that is resistant to reinforcement bar corrosion. Thus, the electrical resistivity of the HES-ECC mixtures may indicate a potential durability issue driven by the presence of flaws and the high-strength binders.

As seen in Fig. 8, electrical resistivities of all mixtures were developed with time which can be attributed to a decrease in the size and quantity of water-filled capillaries as both the size and interconnectivity of the pores reduce as hydration products fill the pores and thus obstruct the electrical current. CAC mixtures were significantly more resistant to electric current than WPC mixtures, although the difference in strength values was not that substantial. In this case, it should also be noted that the electrical resistance also depends on the chemical composition of the pore solution and therefore does not necessarily give results in parallel with other test methods. Especially for CAC at early ages, high resistivity values were obtained ensuring a mixture with high resistivity to chloride penetration and a low possibility of reinforcement corrosion (Shane et al. 1999; ACI 2010). On the other hand, the resistance of WPC mixtures significantly increased continuously at all test ages. However, the development of resistivity was not rapid as CAC which gains most of its strength in a very short time after casting. For both cement types, the use of crumb rubber as an artificial flaw resulted in the highest resistivity which can be attributed to the dielectric nature of the rubber (Kaewunruen and Meesit 2016). Besides, expanded glass also enhanced the electrical resistivity of the mixtures as glass replacement is readily reported to improve the resistivity of cement-based materials in the previous studies (Her-Yung 2009; Kamali and Ghahremaninezhad 2015; Siad et al. 2017). It can be deduced that both of the flaws have potential positive effect on the corrosion protection of high early strength ECC mixtures.

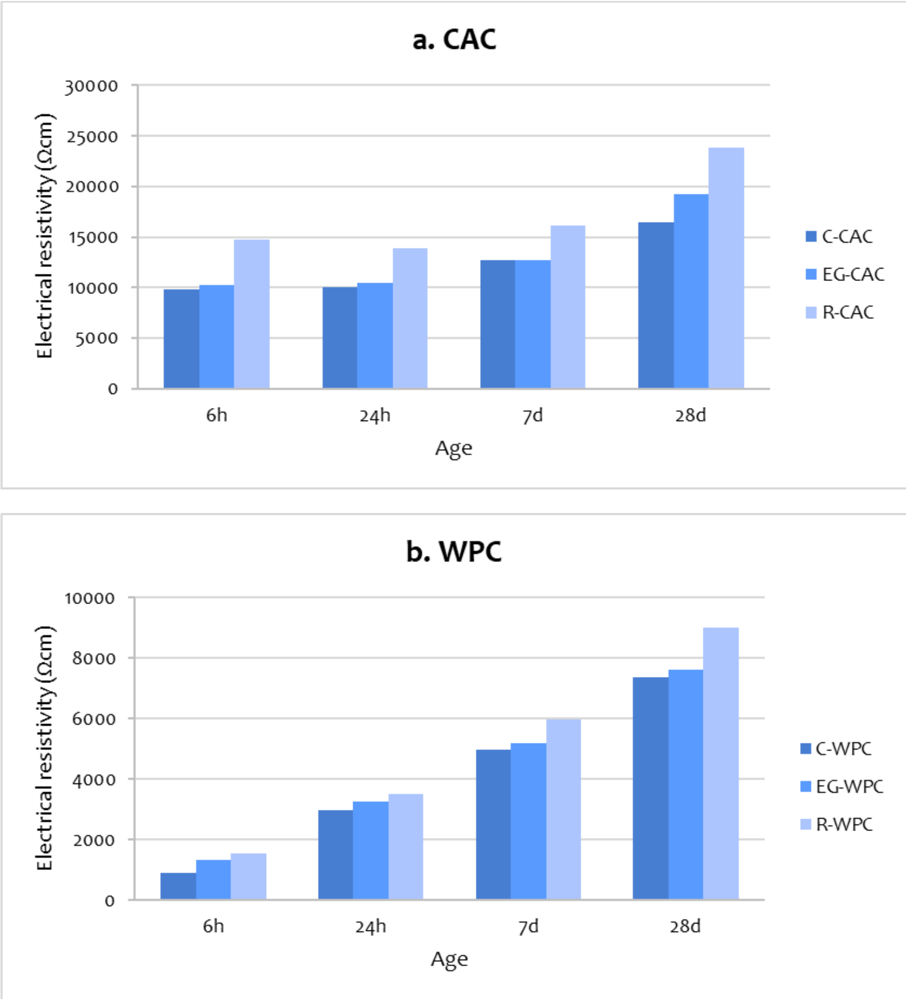

Fig. 8. Electrical resistivities of the mixtures.

4. Conclusions

This study evaluates the utilization of non-portland calcium aluminate cement as a primary binder for high-early strength Engineered Cementitious Composites design and compares it with conventionally used high early strength portland cement in terms of mechanical, abrasion, shrinkage and NDT properties while recycled materials of crumb rubber and expanded glass were employed as artificial flaws to ensure sufficient ductility. The results of the experimental study have led to the following conclusions:

It is possible to produce high early strength ECC mixtures by using both types of cement with a compressive strength well over 30 MPa at 6 hours after casting for the mixtures without any flaws. Calcium aluminate cement mixtures with lithium carbonate mixtures acquired this early strength without eliminating the entire amount of fly ash, while fly ash had to be removed in white portland cement mixtures.

For both cement types, most of the compressive strength was acquired before 24 hours, while the addition of 5% by volume artificial flaws reduced the compressive strength of both control mixtures to a limited extent. Crumb rubber addition resulted in a lower compressive strength compared to expanded glass, yet a satisfactory level of strength can be obtained for both of the flaw types.

Flexural strengths revealed a similar trend with the compressive strength as expected. While the deflection capacity of the control mixtures decreased with time, deflection hardening could be observed at all ages. Although flexural performances were similar for control mixtures at 6 hours, calcium aluminate cement mixtures exhibited higher deformability afterward. Both flaws significantly improved the deformation capacity of the HES-ECC mixtures.

All HES-ECC mixtures became more resistant to abrasion over time. Despite the increase in abrasion depths with the artificial flaws, their effect was minimal.

The drying shrinkages of calcium aluminate cement mixtures were not largely affected by the use of artificial flaws while for white portland cement mixtures, the effect of flaws was more pronounced. It is possible to conclude that the use of expanded glass reduces drying shrinkage for both cement types whereas the rubber particles resulted in an increase. In general, it can be claimed that the shrinkage values do not change in a way that critically increases the cracking potential.

As expected, the UPV and dynamic elastic modulus values increased with age and reduced when artificial flaws were added to the mixtures. Electrical resistivities were improved through the use of artificial flaws due to the low electrical conductivity of the artificial flaws used. Since rubber is a dielectric material, HES-ECC mixtures with rubber crumb exhibited the highest electrical resistance.

In light of all the mechanical, abrasion, shrinkage, and non-destructive testing results, it is evident that high early-strength ECC mixtures produced with calcium aluminate cement are suitable candidates for use in repair purposes. However, it is recommended to also consider the effects of potential effects of phase changes in the long term.

Acknowledgements

Authors gratefully acknowledge Çimsa Mersin Cement Factory, Yatağan Thermal Power Plant, Polisan Construction Chemicals and BASF Chemical Company for their material support.

Funding

The authors received no financial support for the research, authorship, and/or publication of this manuscript.

Conflict of Interest

The authors declared no potential conflicts of interest with respect to the research, authorship, and/or publication of this manuscript.

Author Contributions

All of the authors made substantial contributions to conception and design, or acquisition of data, or analysis and interpretation of data; were involved in drafting the manuscript or revising it critically for important intellectual content; and gave final approval of the version to be published.

Data Availability

The datasets created and/or analyzed during the current study are not publicly available, but are available from the corresponding author upon reasonable request.

References

ACI (2010). ACI 222R-01 Protection of Metals in Concrete against Corrosion Reported by ACI Committee 222. ACI Committee Report. Farmington Hills, MI, USA.

Al-Fakih A, Mohammed BS, Liew MS (2021). On rubberized engineered cementitious composites (R-ECC): A review of the constituent material. *Case Studies in Construction Materials,* 14.

Albano C, Camacho N, Reyes J, Feliu JL, Hernández M (2005). Influence of scrap rubber addition to Portland I concrete composites: Destructive and non-destructive testing. *Composite Structures,* 71(3–4), 439–446.

ASTM C109 (2020). Standard Test Method for Compressive Strength of Hydraulic Cement Mortars (Using 2-in. or [50 mm] Cube Specimens). Annual Book of ASTM Standards (04 vol.). West Conshohocken, PA, USA.

ASTM C215 (1998). Standard test method for fundamental transverse, longitudinal, and torsional resonant frequencies of concrete specimens. Annual Book of ASTM Standards (4 vol.). West Conshohocken, PA, USA.

ASTM C494 (2013). Standard specification for chemical admixtures for concrete. Annual Book of ASTM Standards (04 vol.). West Conshohocken, PA, USA.

ASTM C596 (2007). Standard test method for drying shrinkage of mortar containing hydraulic cement. Annual Book of ASTM Standards (11 vol.). West Conshohocken, PA, USA.

ASTM C597 (2016). Standard test method for pulse velocity through concrete. American Society for Testing and Materials, West Conshohocken, PA, USA.

ASTM C944 (2007). Standard test method for abrasion resistance of concrete or mortar surfaces by the rotating-cutter method. Annual Book of ASTM Standards (99 vol.), West Conshohocken, PA, USA.

Choi Y, Kim IH, Lim HJ, Cho CG (2022). Investigation of strength properties for concrete containing fine-rubber particles using UPV. *Materials,* 15(10).

Emmons PH (1996). Concrete Repair and Maintenance Illustrated: Problem Analysis, Repair Strategy, and Techniques. R.S. Means, Wiley, New Jersey.

Emmons PH, Sordyl DJ (2006). The state of the concrete repair industry, and a vision for its future. *Concrete Repair Bulletin*, 7–14.

EN 14647 (2007). Calcium aluminate cement – Composition, specification and conformity criteria. British Standard (3 vol.).

FHWA (1998). Corrosion Protection: Concrete Bridges. Federal Highway Administration report FHWA-RD-98-088, Virginia, USA.

Frangopol DM, Furuta H (eds) (2001). Life-cycle cost analysis and design of civil infrastructure systems. Life-Cycle Cost Analysis and Design of Civil Infrastructure Systems. Reston, VA: American Society of Civil Engineers.

Her-Yung W (2009). A study of the engineering properties of waste LCD glass applied to controlled low strength materials concrete. *Construction and Building Materials,* 23(6), 2127–2131.

Ideker JH, Scrivener KL, Fryda H, Touzo B (2019). Calcium Aluminate Cements. *In: Hewlett PC, Liska M, editors, Lea's Chemistry of Cement and Concrete*, Butterworth-Heinemann, 537-584.

Huang X, Ranade R, Ni W, Li VC (2013). On the use of recycled tire rubber to develop low E-modulus ECC for durable concrete repairs. *Construction and Building Materials,* 46, 134–141.

Shane JD, Aldea CM, Bouxsein NF, Mason TO, Jenning HM, Shaw SP (1999). Microstructural and pore solution changes induced by rapid chloride permeability test measured by impedance spectroscopy. *Concrete Science and Engineering,* 1(2), 110–119.

Kaewunruen S, Meesit R (2016). Sensitivity of crumb rubber particle sizes on electrical resistance of rubberised concrete. *Cogent Engineering,* 3(1).

Kamali M, Ghahremaninezhad A (2015). Effect of glass powders on the mechanical and durability properties of cementitious materials. *Construction and Building Materials,* 98, 407–416.

Keskin SB, Sahmaran M, Yaman IO, Lachemi M (2014). Correlation between the viscoelastic properties and cracking potential of engineered cementitious composites. *Construction and Building Materials,* 71, 375–383.

Keskin SB, Sulaiman K, Sahmaran M, Yaman IO (2013). Effect of presoaked expanded perlite aggregate on the dimensional stability and mechanical properties of Engineered Cementitious Composites. *Journal of Materials in Civil Engineering,* 25(6), 763–771.

Kim YY, Kong HJ, Li VC (2003). Design of Engineered Cementitious Composite Suitable for Wet-Mixture Shotcreting. *ACI Materials Journal,* 100(6).

Kırca Ö (2006). Temperature Effect on Calcium Aluminate Cement Based Composite Binders. *Ph.D. Thesis,* Middle East Technical University, Ankara, Türkiye.

Kurtz S, Balaguru P, Condolazio G, Maher A (1997). Fast track concrete for construction repair. *Final Report*, Rutgers Department of Civil & Environmental Engineering, The State University, Piscataway, NJ.

Li M, Li VC (2011a). Cracking and healing of engineered cementitious composites under chloride environment. *ACI Materials Journal,* 108(3).

Li M, Li VC (2011b). High-early-strength engineered cementitious composites for fast, durable concrete repair-material properties. *ACI Materials Journal* 108(1), 3–12.

Li VC (1994). From micromechanics to structural engineering – the design of cementitious composites for civil engineering applications. *Structural Engineering/Earthquake Engineering,* 10(2).

Li VC (1997). Engineered cementitious composites (ECC) – tailored composites through micromechanical modeling. *Canadian Society for Civil Engineering*, 1–38.

Li VC (2003). On engineered cementitious composites (ECC). A review of the material and its applications. *Journal of Advanced Concrete Technology,* 1(3).

Li VC (2004). High performance fiber reinforced cementitious composites as durable material for concrete structure repair TT. *Restoration of Buildings and Monuments: an International Journal = Bauinstandsetzen und Baudenkmalpflege: eine Internationale Zeitschrift,* 10(2), 163–180.

Li VC (2012). Tailoring ECC for special attributes: A review. *International Journal of Concrete Structures and Materials* 6(3).

Li VC, Kanda T (1998). Innovations forum: Engineered Cementitious Composites for structural applications. *Journal of Materials in Civil Engineering,* 10(2), 66–69.

Li VC, Mishra DK, Naaman AE, Wight JK, LaFave JM, Wu HC, Inada Y (1994). On the shear behavior of engineered cementitious composites. *Advanced Cement Based Materials,* 1(3), 142–149.

Li VC, Wang S, Wu C (2001). Tensile strain-hardening behavior or polyvinyl alcohol engineered cementitious composite (PVA-ECC). *ACI Materials Journal,* 98(6), 483–492.

Lim YM, Li VC (1997). Durable repair of aged infrastructures using trapping mechanism of engineered cementitious composites. *Cement and Concrete Composites,* 19(4), 373–385.

Marie I (2016). Zones of weakness of rubberized concrete behavior using the UPV. *Journal of Cleaner Production,* 116, 217–222.

Parker F, Lee Shoemaker W (1991). PCC pavement patching materials and procedures. *Journal of Materials in Civil Engineering,* 3(1), 29–47.

Preetha R, Kumari K, Sakthi B, Harikumar CN, Abdul Gani HI (2023). Cause of distress of an old building through analytical and micro–analytical methods – a case study. *Challenge Journal of Concrete Research Letters*, 14(1), 18-30.

Qian S, Li VC (2007). Simplified inverse method for determining the tensile strain capacity of strain hardening cementitious composites. *Journal of Advanced Concrete Technology*, 5(2), 235–246.

Raupach M (2006). Concrete repair according to the new European Standard EN 1504. *Proceedings of the International Conference on Concrete Repair, Rehabilitation and Retrofitting*, ICCRRR 2005.

Şahmaran M, Li VC (2009). Durability properties of micro-cracked ECC containing high volumes fly ash. *Cement and Concrete Research* 39(11).

Şahmaran M, Li VC (2010). Engineered Cementitious Composites. *In Banthia N, Uomoto A, Bentur A, Shah S. P. (eds), Transportation Research Record: Journal of the Transportation Research Board (2164 vol.)*, 1–8. Vancouver: The University of British Columbia, Canada.

Şahmaran M, Al-Emam M, Yıldırım G, Şimşek YE, Erdem TK, Lachemi M (2015). High-early-strength ductile cementitious composites with characteristics of low early-age shrinkage for repair of infrastructures. *Materials and Structures/Materiaux et Constructions,* 48(5), 1389–1403.

Siad H, Lachemi M, Sahmaran M, Mesbah HA, Hossain KMA, Ozsunar A (2017). Potential for using recycled glass sand in engineered cementitious composites. *Magazine of Concrete Research,* 69(17), 905–918.

Soltan DG, Li VC (2018). A self-reinforced cementitious composite for building-scale 3D printing. *Cement and Concrete Composites,* 90, 1-13.

Spragg RP, Bu Y, Snyder KA, Bentz DP, Weiss J (2013). Electrical Testing of Cement-Based Materials: Role of Testing Techniques, Sample Conditioning, and Accelerated Curing. Joint Transportation Research Program.

Tarhan İH, Uysal H (2024). Strengthening of historic masonry vaults with CFRP prepreg. *Challenge Journal of Structural Mechanics*, 10(1), 1-6.

Wang S, Li VC (2006). High-early-strength engineered cementitious composites. *ACI Materials Journal,* 103(2), 97–105.

Whiting D, Nagi M (1994). Strength and durability of rapid highway repair concretes. *Concrete International,* 16(9), 36–41.

Wilson TP, Smith KL, Romine AR (1999). Materials and Procedures for Rapid Repair of Partial-depth Spalls in Concrete Pavements-Manual of Practice. *Federal Highway Administration*.

Woudhuysen J, Abley I (2004). Why is Construction so Backward? Willey Academy, Chichester, UK.

Yang E, Li VC 2007. Numerical study on steady-state cracking of composites. *Composites Science and Technology,* 67(2), 151–156.

Ye J, Hu S, Wang F, Zhou Y, Liu Z (2006). Effect of pre-wetted lightweight aggregate on internal relative humidity and autogenous shrinkage of concrete. *Journal Wuhan University of Technology, Materials Science Edition,* 21(1), 134–137.

Yildirim G, Şahmaran M, Al-Emam MKM, Hameed RKH, Al-Najjar Y, Lachemi M (2015). Effects of compressive strength, autogenous shrinkage, and testing methods on bond behavior of high-early-strength engineered cementitious composites. *ACI Materials Journal,* 112(3), 409–418.

Yokota H, Rokugo K, Sakata N (2008). Recommendations for design and construction of high performance fiber reinforced cement composites with multiple fine cracks. The Japan Society of Civil Engineers, Tokyo.

Yunovich M, Thompson NG (2003). Corrosion of highway bridges: economic impact and control methodologies. *Concrete International,* 25(1), 52–57.

CHALLENGE JOURNAL OF CONCRETE RESEARCH LETTERS 15 (4) (2024) 134–141

Challenge Journal of Concrete Research Letters

Research Article

Optimum design of reinforced concrete beam sections with JAYA algorithm

Yasin Duysak [a], Sinan Melih Nigdeli [a,*], Gebrail Bekdaş [a]

[a] *Department of Civil Engineering, İstanbul University-Cerrahpaşa, 34320 İstanbul, Türkiye*

ABSTRACT

Section design is an important process for designing reinforced concrete structures because of the existence of factors such as bearing capacity and cost. After defining the initial cross sections for reinforced concrete elements, reinforcement amounts are calculated within the framework of certain rules and regulations. In the classical method, optimum cost and reliable structure can be designed by trial and error. Designing with the classical method is quite time-consuming. As in different fields, metaheuristic algorithms are employed to civil engineering applications to reach the optimum solution. In this study, unlike other examples from the literature, the optimum cost design of reinforced concrete beam cross-section was done, adding torsional moment to bending moment and effects of shearing force through the use of the JAYA algorithm. The optimum cost design of a reinforced concrete beam section under the effects of torsional moment, bending moment and shear force is performed. The design is done according to the rules specified in ACI 318 (Building code requirements for structural concrete), as it is well-known and used in many international projects. For the purpose of this study, cross-sections of 10 different reinforced concrete beam cross-sections were designed under 5 different loads for 2 different concrete classes through MATLAB software, with the aim of finding the optimum beam cross-section. A reinforced concrete beam is designed under different torsional loads and for different concrete classes and it is aimed to find the optimum beam cross-section. It shows the effect of torsional force on reinforced concrete beam cross section and reinforcement by using different torsional loads. It was observed that the algorithm used tends to approach the optimum result, increasing the area of concrete with lower unit cost or reducing the distance between stirrups. It was concluded that Jaya algorithm performs effectively with respect to optimizing reinforced concrete beams. The algorithm used can be applied to different reinforced concrete elements.

ARTICLE INFO

Article history:
Received 27 May 2024
Revised 25 July 2024
Accepted 19 August 2024

Keywords:
Beam section
Jaya algorithm
Section optimization
Torsional moment

This is an open access article distributed under the CC BY licence.
© 2024 by the Authors.

1. Introduction

The design of reinforced concrete structural elements is a complex and important process in engineering practice. In this process, civil engineers determine various initial element sizes in structural design and these sizes form the basic reference points for reinforcement design. One of the important objectives of the engineer is to solve the design economically. However, the first choice does not always guarantee an economical design because factors such as economic design, durability and safety of the structure must be considered. Therefore, it is important to experiment with different element sizes to get a better design. It is important to know about the behaviors of engineering structure elements. Studies were conducted in connection with behaviors of structure elements in many fields. El-Sayed and Shaheen (2020) experimentally and analytically examined the behaviors of reinforced concrete beams containing recycled steel fiber and recycled wheat straw ash-based geo-

* *Corresponding author*. Tel.: +90-212-473-7070 ; E-mail address: melihnig@iuc.edu.tr (S. M. Nigdeli)
ISSN: 2548-0928 / DOI: https://doi.org/10.20528/cjcrl.2024.04.003

polymer. El-Sayed (2019) conducted a study on increasing beams' resistance strengths through the addition of industrial lathe wastes to reinforced concrete beams. Ghali et al. (2024) conducted a research examining the behavior of beams with reinforced concrete rectangular beams as reinforced with metallic and non-metallic fibers.

For an experienced engineer, several factors influence the economic design of reinforced concrete elements. These factors include various elements such as material properties of the structural elements, load carrying, structural integrity and aesthetics. However, it is not possible to try thousands of different combinations of sizes with the classical method of trial and error. Therefore, a process called optimization is used to find the best design that satisfies all design constraints. Optimum design methods have been proposed for different reinforced concrete elements and it is possible to apply these methods by using mathematical methods. Some methods have been developed for the optimum solution of engineering problems. Among these methods, optimization algorithms have an important place. Therefore, metaheuristic algorithms are a suitable option to perform a practical optimization. Metaheuristic algorithms are used to solve complex optimization problems by combining different search strategies and algorithm techniques. These algorithms can be tuned to suit the solution of a specific problem and are usually implemented through computer-based software. Thus, it may be possible to obtain optimum designs in large and complex reinforced concrete construction projects.

Consequently, the design of reinforced concrete elements is carried out with a combination of both engineering skill and mathematical optimization techniques. In this process, using an experienced engineering approach and appropriate optimization methods, it is possible to build economical, durable and safe structures. This can save cost and time in building projects, while at the same time improving the performance and quality of the structures.

Many heuristic and metaheuristic algorithms are used in civil engineering. One of the metaheuristic algorithms used in civil engineering is the artificial bee colony (ABC) algorithm. Jahjouh et al. (2013) in the optimal cost design of continuous beams. Tapao and Cheerarot (2017) used artificial bee colony (ABC) algorithm in cost design of reinforced concrete frame systems, Sönmez (2011) in weight minimization and optimum cost design of truss systems, Öztürk and Durmuş (2013) in optimum cost design of reinforced concrete columns.

Çakıroğlu et al. (2021a) conducted a study on the stacking of composite laminates with carbon fiber reinforcement with harmony search algorithm. Çakıroğlu et al. (2020a) used harmony search algorithm for the design of connection slabs under effect of cutting twisting and lateral twisting torsion and tried to find minimum cross-section areas that are to meet lateral torsion twisting loan and cutting tensions and to reduce the cost. Çakıroğlu et al. (2020b) used harmony search algorithm in order to find the highest possible twisting load, keeping the cost and weight of rectangular laminated composite plates at a minimum. Çakıroğlu et al. (2021b) made use of harmony search algorithm to reduce CO_2 emission which also offers the best performance in the design of steel columns with concrete filling. Bekdaş et al. (2022a) used harmony search algorithm for optimum design of cylindrical walls and created a database using 7744 samples and machine learning models were developed based on such database. Bekdaş et al. (2022b) prepared 3125 different data samples for the design of reinforced concrete circular columns and for their optimum cost and ensured that machine learning models focusing on data were developed. Çakıroğlu et al. (2023a) created 40569 data sets using harmony search algorithm for the design of console shoring retaining walls and worked on machine learning techniques.

Another algorithm used in the optimal design of reinforced concrete elements is the teaching-learning based optimization (TLBO) algorithm, which is inspired by the two different stages of training developed by Rao et al. (2011). Kayabekir et al. (2020), Temur and Bekdaş (2016), Bekdaş and Temür (2017), and Öztürk et al. (2020) used the teaching-learning based optimization (TLBO) algorithm for the design and cost optimization of retaining walls; Niğdeli et al. (2018) for the design and optimum cost of reinforced concrete single foundations, Dede and Ayvaz (2015) for shape and size optimization of truss systems and elements, Bekdaş and Niğdeli (2016) for cost optimization of reinforced concrete columns of different heights.

Another algorithm used in structural optimization is the genetic algorithm (GA) developed from evolutionary theory (GA) (Goldberg and Samtani 1986). Guimarães et al. (2022) in the optimal design of concrete-filled composite columns; Rao and Babu (2006) in the cost optimization design of short columns by combining with artificial neural network method; Pierott et al. (2021), Yousif and Najem (2013), Deliktaş et al. (2009), and Govindaraj and Ramasamy (2005) in the cost design of reinforced concrete simply supported and continuous beams; Alqedra et al. (2011) in the design of reinforced concrete prestressed beams; Sahab et al. (2005) and Nimtawat and Nanakorn (2010) in the design of slabs; Shooli et al. (2019) and Mergos (2021) in the optimal cost design of reinforced concrete frames; Dos Santos et al. (2023) analyzed the cost and CO_2 emission of reinforced concrete beams with the help of genetic algorithm. The Jaya algorithm, which is also used in this study, has not been studied in the field of civil engineering. Öztürk et al. (2020) used Jaya algorithm for cost and design optimization on retaining walls and Yücel et al. (2023) used Jaya algorithm to minimize the weight of steel truss systems of different sizes. Kaveh and Hamedani (2023) compared the results of certain examples from the literature against the hybrid set-theoretical Jaya algorithm (ST-JA) classic Jaya algorithm and other metaheuristic algorithms because of classic Jaya algorithm's likelihood of early convergence and getting stranded in the local optimum under certain circumstances. They revealed that convergence speed and results performed better based on numerical results when compared to ST-JA classic Jaya algorithm and other metaheuristic algorithms. Pham and Nguyen (2024) took advantage of a Jaya-based optimization algorithm demonstrated to be innovative for the analysis of fuzzy displacements of two-dimensional and 3D cage beams under static loads. Du et al. (2018) conducted a study intended to determine sites of damage at structures and their scope, using Jaya algorithm. Çakıroğlu et al. (2023b) used Jaya algorithm and Manta Ray Foraging Optimization in order to ascertain optimal cross-section dimensions of steel pipe columns with concrete filling and minimize CO_2. Dede (2018) used Jaya algorithm to conduct analysis and optimal design of design and steel grillage structures and concluded that Jaya algorithm was effective in the analysis of steel grillage structures.

In this study, the Jaya algorithm developed by Rao (2016) is used for the optimum design of reinforced concrete beam sections under the effect of shear force, moment force and torsional force. Different torsional moment effects are considered to see the effect of the torsional moment on the reinforced concrete beam section. As part of this study, 5 different torsional moment sizes were used for 10 different beam designs. For the purpose of design of reinforced concrete cross-section, design restrictions and building rules specified in ACI 318 (Building Code Requirements for Structural Concrete) regulation were taken into account and two different concrete classes; i.e. C30 and C35, were used for the design of beam cross-sections.

2. Methodology

Jaya algorithm is a population-based algorithm composed of a single part and it is an algorithm that is easier to use when compared to algorithms made of 2 phases such as teaching- and learning-based optimization algorithms used prevalently in the field of civil engineering, flower pollination algorithm, harmony search algorithm, genetic algorithm and differential evolution algorithm. In Jaya algorithm, design variables are randomly assigned and the algorithm works on the principle of moving away from the worst solution and converging to the best solution. The algorithm determines, at the first phase, the best and the worst values at the population, and each new solution is updated so that it remains between the best and the worst solutions, then the updated solution is evaluated based on updated design restrictions, the best solution is chosen. The process continues via iterations. The process is terminated when it reaches a certain number of iterations or appropriate values. The equation of the one-part algorithm is shown in Eq. (1) below.

$$x_i^{j,t+1} = x_i^{j,t} + r_1(x_i^{*} - |x_i^{j,t}|) - r_2(x_i^{w} - |x_i^{j,t}|)$$
$$i=1, 2, \ldots, n \; ; j=1, 2, \ldots, p \; ; t=1, 2, \ldots, t_{\max} \qquad (1)$$

In Eq. (1), (x_i^*) is the best available solution and (x_i^w) is the worst available solution. In the formula, r_1 and r_2 are random numbers between 0 and 1. $r_1(x_i^*-|x_i^{j,t}|)$ portion of the equation ensures that the solution converges to the best result whereas the term $r_2(x_i^w-|x_i^{j,t}|)$ makes sure that the solution gets away from the worst result. Real numbers r_1 and r_2, randomly created in the equation, ensure that design space is more effectively inspected while absolute value $|x_i^{j,t}|$ further increases the search capability of the algorithm. The Jaya algorithm compares its results with each other in the current solution and continues by updating itself to find the better solution in the next solution. This process continues until the stopping criterion is met. The stopping criterion is usually constrained by a result threshold or number of iterations. The flowchart about Jaya algorithm is given in Fig. 1.

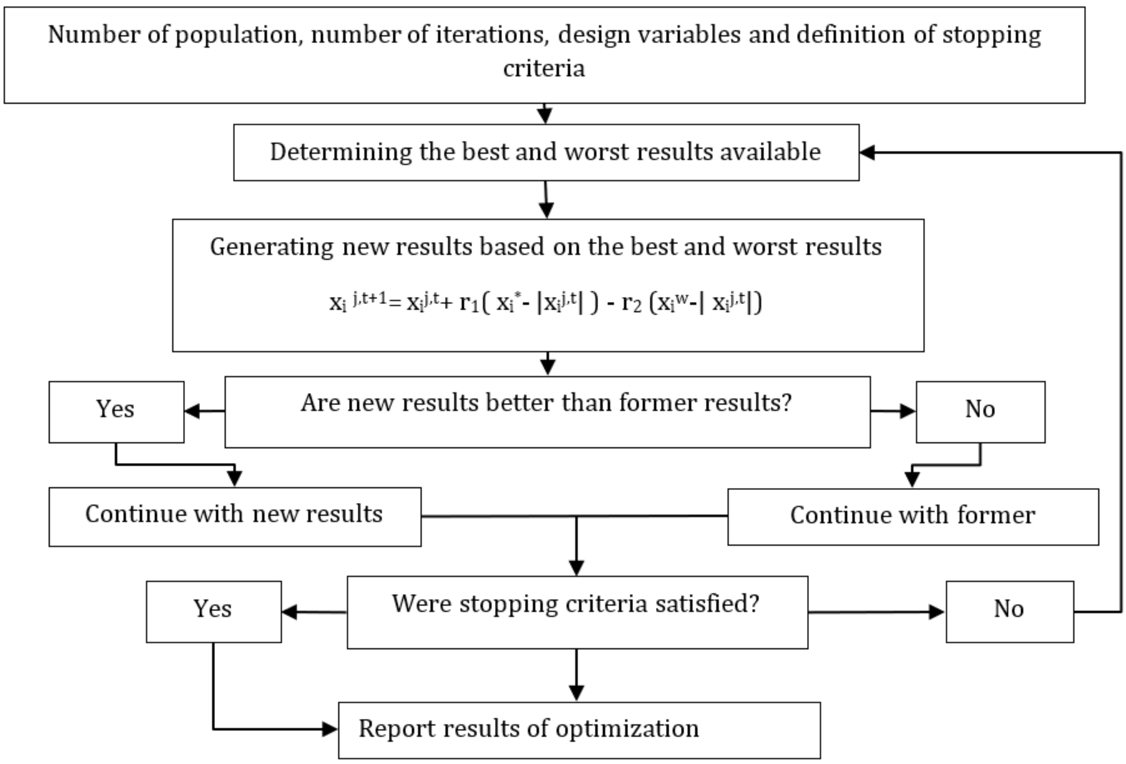

Fig. 1. Flow chart of the optimization method.

One of the basic requirements of engineering optimization algorithms is to clearly define the problem. This process involves the identification of the problem data, design variables, definition of the design constraints and the determination of the parameters of the algorithm. The design constants and design variables are shown in Table 1. In reinforced concrete beam optimization, the design variables are width (b_w), height (h), area of longitudinal reinforcement, size of shear reinforcement and spacing of shear reinforcement. A cross-section of the beam design is shown in Fig. 2.

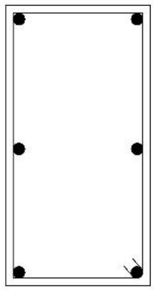

Fig. 2. Details of beam cross-section and reinforcement.

Table 1. Design variables and design constants.

Explanation	Symbol	Unit	Value
Beam width	h	mm	250–400
Beam depth	b	mm	350–600
Compressive strength of concrete	f_{ck}	MPa	30–35
Yield strength of steel	f_{yk}	MPa	420
Modulus of elasticity	E	MPa	27800
Specific density of concrete	γ_c	t/m^3	2.5
Specific density of steel	γ_s	t/m^3	7.86
Concrete cover	d'	mm	40
Stirrup	Ø	mm	8–14

Since ACI 318 is used as a reference for reinforced concrete design in international projects and many countries have adopted ACI 318 directly, this study considers ACI 318 (Building code requirements for structural concrete and commentary) for design constraints and construction rules.

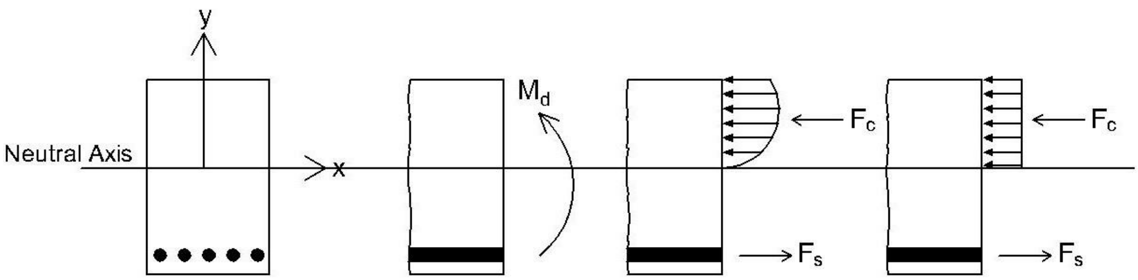

Fig. 3. Assumption of the equivalent load distribution.

As shown in Fig. 3, the resultant force forming in the concrete pressure region in the upper part of the neutral axis is called F_c whereas the resultant force forming in the tensile region in the lower part of the neutral axis is called F_s.

$$F_c = 0.85 \cdot f'_c \cdot b \cdot a \quad (2)$$

In Eq. (2), concrete compressive strength was multiplied by 0.85 and a indicates equivalent pressure block depth.

$$a = \beta_1 \cdot c \quad (3)$$

where c is the depth of the neutral axis in the pressure region. At ACI 318, β_1 represents a rectangular pressure block, which is shown in Eq. (4).

$$\beta_1 = 0.85 \quad 17 \text{ MPa} < f'_c < 28 \text{ MPa}$$

$$\beta_1 = 0.85 - 0.0071428\,(f'_c - 28) \quad f'_c > 28 \text{ MPa} \quad (4)$$

The resultant tensile force occurring in the tensile region is shown in Eq. (5).

$$F_s = A_s \cdot f_y \quad (5)$$

where A_s means the reinforcement region. A balanced breakage occurs when concrete unit shortening (ε_c) reaches concrete ultimate unit shortening (ε_c=0.003), and unit shortening of tensile reinforcement (ε_y) reaches the yield strength of the reinforcement at the same time. According to ACI 318, breakage in beams must be designed according to sub-equilibrium breakage. Calculations for sub-equilibrium breakage are calculated according to the balanced reinforcement ratio.

Balanced reinforcement ratio ρ_b is calculated with the following equation based on form changing status shown in Fig. 4 with known material characteristics and dimensions.

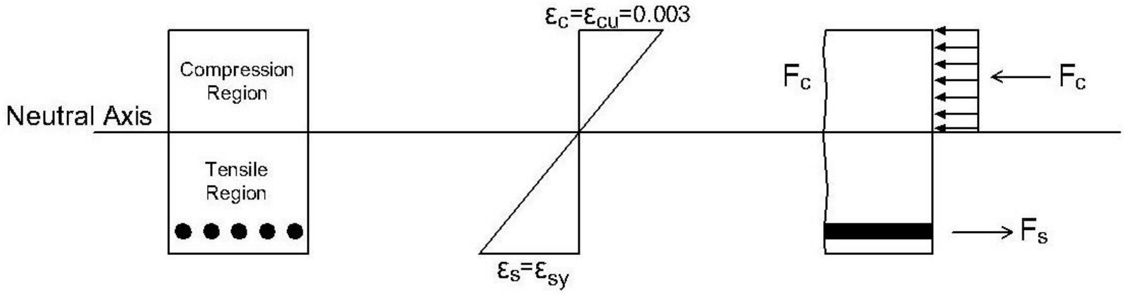

Fig. 4. Internal forced forming in the beam cross-section.

$$\rho_b = 0.85 \cdot \beta_1 \frac{f'_c}{f_y}\left(\frac{600}{600+f_y}\right) \quad (6)$$

The maximum reinforcement ratio (ρ_{max}) must not be higher than 0.75 times the balanced reinforcement and the maximum reinforcement ratio (ρ_{max}) must be lower than the value 0.025 for beams to demonstrate ductile behavior.

In ACI 318, the minimum longitudinal reinforcement ratio of beams is calculated as shown in Eqs. (7) and (8).

$$A_{s,\min} \geq \frac{\sqrt{f'_c}}{4f_y}\, b \cdot d \quad (7)$$

$$A_{s,\min} \geq \frac{1.4}{f_y}\, b \cdot d \quad (8)$$

If reinforcement ratios so calculated are lower than the minimum conditions specified in Eqs. (7) and (8), the ratio of minimum longitudinal reinforcement will be taken into account. If the longitudinal reinforcement ratio proves to be higher than the maximum reinforcement ratio, the dimensions of the cross-section are changed and calculations are repeated. Once reinforcements about the beam are calculated, the stirrup design is done. Rules and restrictions of required regulation for the design of stirrup should satisfy the following requirements;

Shearing strength provided by concrete;

$$V_c = 0.17\sqrt{f'_c}\, b \cdot d \quad (9)$$

Shearing strength provided by reinforcement;

$$V_s = 0.67\sqrt{f'_c}\, b \cdot d \quad (10)$$

Minimum shearing reinforcement region;

$$A_{v,\min} = 0.35\, \frac{b_w s}{f_{yt}} \quad (11)$$

where s refers to the distance between stirrup reinforcements. Distance between shearing reinforcements;

$$s \leq \begin{cases} d/4 \\ 8\phi_{min} \\ 150 \text{ mm} \end{cases} \quad (12)$$

The existence of a torsional moment in a structure system is a mandatory condition, this is called conformity torsion and hyperstatic systems generally have conformity torsion. Torsional moment load to shearing tensions and shearing reinforcements are used at elements to meet such tensions. According to ACI 318, if shearing force and conformity torsional have an impact at the same time, rules and restrictions introduced by the regulation are shown in the equations below.

Dimension check of the required cross-section is carried out according to Eqs. (13) and (14) to be able to keep diagonal cracks driven by torsional moment under control.

$$\frac{T}{S} + \frac{V}{b_w d} \leq 0.22\, f_{cd} \quad (13)$$

$$\sqrt{\left(\frac{V}{b_w d}\right)^2 + \left(\frac{T p_h}{1.7A_{oh}^2}\right)^2} \leq \varnothing\left(\frac{V_c}{b_w d} + 0.66\sqrt{f'_c}\right) \quad (14)$$

In Eq. (14), T means torsional moment, p_h perimeter of cross-section remaining between reinforcements whereas A_{oh} means the area remaining between corner reinforcements, V_c means shearing force and $\varnothing$ means reduction coefficient.

Calculation of torsion stirrup;

$$A_t = \frac{T\, s}{2\varnothing A_o f_{yt} cot\theta} \quad (15)$$

Calculation of shearing reinforcement;

$$A_v = \frac{V\, s}{f_{yt} d} \quad (16)$$

The value calculated for the torsion stirrup in Eq. (15) is for one arm of the stirrup whereas the value calculated in Eq. (16) is for two arms of the stirrup. The total area of the stirrup area is shown in Eq. (17).

$$A_{v+t} = A_v + 2A_t \quad (17)$$

Distance between stirrups for elements under the effect of both torsional effect and shearing effect should not exceed conditions specified in Eq. (18).

$$s \leq \begin{cases} d/2 \\ {}^{ue}/_{8} \\ 300 \text{ mm} \end{cases} \quad (18)$$

The total area of closed stirrup arms for elements under the effect of both the torsional effect and shearing effect is shown in Eq. (19).

$$A_v + 2A_t = 0.062\sqrt{f'_c}\frac{b_w s}{f_{yt}} \geq 0.35\frac{b_w s}{f_{yt}} \quad (19)$$

The minimum longitudinal reinforcement area for the torsional moment is shown in Eq. (20).

$$A_l = \frac{A_t}{s} p_h \frac{f_{yt}}{f_y} cot^2\theta \quad (20)$$

3. Numerical Example

In this study, the sizing and reinforcement of 10 different reinforced concrete beam sections were optimized. The external loads consist of shear force, bending moment and torsional moment as shown in Fig. 5. Different torsional moments are applied on the section and the effect of torsional moment on the beam section size and reinforcement is investigated.

The shear force and bending moment acting on the section are taken as 100 kN and 100 kNm, respectively. The torsional moment was taken as 10, 20, 30, 40, and 50 kNm. The external loads acting on the beam section and the concrete classes used in the beam section are shown in Table 2. Table 2 shows 10 different beam cross-sections. 100 kN bending moment of shearing force having an impact upon the beam cross-section was selected as 100 kNm and remained stable at all samples, torsional moment and concrete classes were changed and their impact upon the concrete cross-section was examined. In Table 2, *B* shows that the cross-section is a beam and the numerical value shows the torsional moment having an impact upon the beam whereas *L* shows the concrete compressive strength is 30 MPa and *H* shows concrete compressive strength is 35 MPa.

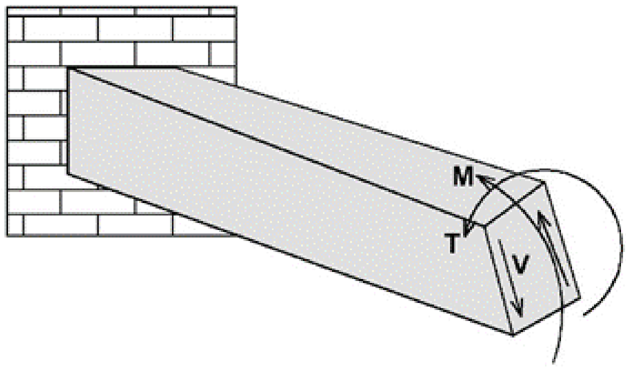

Fig. 5. Loads acting on the beam section.

Table 2. Sectional effects and concrete classes.

Sample number	Shear force (*kN*)	Bending moment (*kNm*)	Torsional moment (*kNm*)	Concrete class
B10L	100	100	10	C30
B10H	100	100	10	C35
B20L	100	100	20	C30
B20H	100	100	20	C35
B30L	100	100	30	C30
B30H	100	100	30	C35
B40L	100	100	40	C30
B40H	100	100	40	C35
B50L	100	100	50	C30
B50H	100	100	50	C35

Conducting an optimization study by adding a torsional moment of differing sizes to a beam cross-section was tried for the first time with this study and 10 different beam cross-sections were designed according to ACI 318 regulation, using Jaya algorithm. In addition to different torsional moments, 2 different concrete classes were used in the beam cross-section. In respect of sample numbering in Table 2, *B* indicates that the element is a beam, numbers at the middle part indicate the torsional moment having an impact upon beam cross-section, cross-section *L* indicates that the class of concrete used is C30, and *H* indicates that the class of concrete used in the cross-section is C35. Table 3 shows varying torsional moment and bending reinforcement area of samples of beam designed according to concrete classes, body reinforcement area, diameter and range of stirrup and dimensions of beam cross-section.

A total of 10 beam sections are studied in the study and the optimum results are given in Table 3.

4. Conclusions

Unlike existing studies from the literature, the effect of torsional moment was examined in this study. The optimum values of reinforced concrete beam sections are analyzed with the help of Jaya algorithm. The effect of torsional moment is seen by examining the optimum beam section results. As the torsional moment increases, the cross section and body reinforcement of the beam increases and the stirrup spacing decreases. In the first phase, the algorithm increases the cross-section area since the unit cost of the concrete is lower than the unit cost of the reinforcement. In a case satisfying minimum material cost, the algorithm increases cross-section height (h), from among dimensions of cross-section, at beams whereas cross-section width (b_w) makes sure that it remains at minimum limit, where possible. An increase in torsional moment increases the area of longitudinal reinforcement at the beam cross-section and reduces the ranges of stirrups. The Jaya algorithm used in the study is found to be effective in finding the optimum values of the beam cross-section. Jaya algorithm is a suitable algorithm for solving optimization problems of reinforced concrete elements. It is considered to be usable for other reinforced concrete elements or systems. The ability to design reinforced concrete elements under many load combinations in a very short time through optimization algorithms will save a great deal of time for engineers. Structures built using optimum cross-sections will enable us to use our world's limited resources more efficiently.

Table 3. Optimization results.

Sample number	Concrete class	Torsional moment (kNm)	Flexural reinforcement (mm^2)	Web reinforcement *(mm^2)*	Stirrup (d/s)	Section (b_w/h) (mm)
B10L	C30	10 kNm	538.35	308.62	Ø8/147.5	250/500
B10H	C35	10 kNm	535.18	308.62	Ø8/147.5	250/500
B20L	C30	20 kNm	481.85	598.32	Ø8/99.1	250/550
B20H	C35	20 kNm	479.59	598.32	Ø8/103.6	250/550
B30L	C30	30 kNm	481.85	897.48	Ø8/67.9	250/550
B30H	C35	30 kNm	479.59	897.48	Ø8/69.9	250/550
B40L	C30	40 kNm	534.66	1034.75	Ø8/60.7	300/500
B40H	C35	40 kNm	532.08	1034.75	Ø8/62.7	300/500
B50L	C30	50 kNm	534.66	1293.40	Ø8/50.0	300/500
B50H	C35	50 kNm	532.08	1293.40	Ø8/50.1	300/500

Acknowledgements

None declared.

Funding

The authors received no financial support for the research, authorship, and/or publication of this manuscript.

Conflict of Interest

The authors declared no potential conflicts of interest with respect to the research, authorship, and/or publication of this manuscript.

Author Contributions

All of the authors made substantial contributions to conception and design, or acquisition of data, or analysis and interpretation of data; were involved in drafting the manuscript or revising it critically for important intellectual content; and gave final approval of the version to be published.

Data Availability

The datasets created and/or analyzed during the current study are not publicly available, but are available from the corresponding author upon reasonable request.

References

ACI 318-05 (2008). Building code requirements for structural concrete (ACI 318-05) and commentary. ACI Committee, American Concrete Institute, USA.

Alqedra M, Arafa M, İsmail M (2011). Optimum cost of prestressed and reinforced concrete beams using genetic algorithms, *Journal of Artificial Intelligence*, 4(1), 76-88.

Bekdaş G, Çakıroğlu C, İslam K, Kim S, Geem ZW (2022a). Optimum design of cylindrical walls using ensemble learning methods. *Applied Sciences*, 12, 2165.

Bekdaş G, Çakıroğlu C, Kim S, Geem ZW (2022b). Optimization and predictive modeling of reinforced concrete circular columns. *Materials*, 15, 6624.

Bekdaş G, Niğdeli SM (2016). Optimum design of reinforced concrete columns employing teaching-learning based optimization. *Challenge Journal of Structural Mechanics,* 2(4), 216-219.

Bekdaş G, Temür R (2017). Metaheuristic approaches for optimum design of cantilever reinforced concrete retaining walls. *Challenge Journal of Structural Mechanics*, 3(1), 23-30.

Çakıroğlu C, Bekdaş G, Kim S, Geem ZW (2020a). Optimisation of shear and lateral–torsional buckling of steel plate girders using metaheuristic algorithms. *Applied Sciences*, 10, 3639.

Çakıroğlu C, Bekdaş G, Geem ZW (2020b). Harmony search optimisation of dispersed laminated composite plates. *Materials*, 13, 2862.

Çakıroğlu C, İslam K, Bekdaş G, Kim S, Geem ZW (2021a). Metaheuristic optimization of laminated composite plates with cut-outs. *Coatings*, 11, 1235.

Çakıroğlu C, İslam K, Bekdaş G, Kim S, Geem ZW (2021b). CO_2 emission optimization of concrete-filled steel tubular rectangular stub columns using metaheuristic algorithms. *Sustainability*, 13, 10981.

Çakıroğlu C, İslam K, Bekdaş G, Nehdi ML (2023a). Data-driven ensemble learning approach for optimal design of cantilever soldier pile retaining walls. *Structures*, 51, 1268-1280.

Çakıroğlu C, İslam K, Bekdaş G (2023b). Manta Ray Foraging and Jaya Hybrid Optimization of concrete filled steel tubular stub columns based on CO_2 emission. *Hybrid Metaheuristics in Structural Engineering*, 480, 111-125.

Dede T (2018). Jaya algorithm to solve single objective size optimization problem for steel grillage structures. *Steel and Composite Structures*, 26(2), 163-170.

Dede T, Ayvaz Y (2015). Combined size and shape optimization of structures with a new meta-heuristic algorithm. *Applied Soft Computing*, 28, 250-258.

Deliktaş B, Bikçe M, Coşkun H, Türker HT (2009). Betonarme kirişlerin optimum tasarımında genetik algoritma parametrelerinin etkisinin belirlenmesi. *Fırat University Journal of Engineering Science*, 21(2), 125-132. (in Turkish)

Dos Santos NR, Alves EC, Kripka M (2023). Towards sustainable reinforced concrete beams: multi-objective optimization for cost, CO_2 emission, and crack prevention. *Asian Journal of Civil Engineering*, 25, 575-582.

Du DC, Vinh HH, Trung VD, Quyen NTH, Trung NT (2018). Efficiency of Jaya algorithm for solving the optimization-based structural damage identification problem based on a hybrid objective function. *Engineering Optimization*, 50(8), 1233-1251.

El-Sayed TA (2019). Flexural behavior of RC beams containing recycled industrial wastes as steel fibers. *Construction and Building Materials*, 212, 27-38.

El-Sayed TA, Shahen YBI (2020). Flexural performance of recycled wheat straw ash-based geopolymer RC beams and containing recycled steel fiber. *Structures*, 28, 1713-1728.

Ghali MKN, El-Sayed TA, Salah A, Khater N (2024). Performance of RC beams under shear loads strengthened with metallic and non-metallic fibers. *Buildings*, 14, 1869.

Goldberg DE, Samtani MP (1986). Engineering optimization via genetic algorithm. *Proceedings of Ninth Conference on Electronic Computation,* ASCE, New York, United States of America, 471-482.

Govindaraj V, Ramasamy JV (2005). Optimum detailed design of reinforced concrete continuous beams using Genetic Algorithms. *Computers & Structures*, 84(1-2), 34-48.

Guimarães SA, Klein D, Calenzani AFG, Alves EC (2022). Optimum design of steel columns filled with concrete via genetic algorithm: environmental impact and cost analysis. *International Engineering Journal*, 75(2), 117-128.

Jahjouh MM, Arafa MH, Alqedra MA (2013). Artificial Bee Colony (ABC) algorithm in the design optimization of RC continuous beams. *Structural and Multidisciplinary Optimization*, 47, 963-979.

Kaveh A, Hamedani KB (2023). Discrete structural optimization with set-theoretical Jaya algorithm. *Iranian Journal of Science and Technology, Transactions of Civil Engineering*, 47, 79-103.

Kayabekir AC, Yücel M, Bekdaş G, Nigdeli SM (2020). Comparative study of optimum cost design of reinforced concrete retaining wall via metaheuristics. *Challenge Journal of Concrete Research Letters*, 11(3), 75-81.

Nigdeli SM, Bekdaş G, Yang X-S (2018). Metaheuristic optimization of reinforced concrete footings. *KSCE Journal of Civil Engineering*, 22, 4555-4563.

Nimtawat A, Nanakorn P (2010). A genetic algorithm for beam–slab layout design of rectilinear floors. *Engineering Structures*, 32(11), 3488-3500.

Özturk HT, Durmus A (2013). Optimum cost design of RC columns using artificial bee colony algorithm. *Structural Engineering and Mechanics*, 45(5), 643-654.

Öztürk HT, Dede T, Türker E (2020). Optimum design of reinforced concrete counterfort retaining walls using TLBO, Jaya algorithm. *Structures*, 25, 285-296.

Pham HA, Nguyen B D (2024). Fuzzy structural analysis using ımproved Jaya-based optimization approach. *Periodica Polytechnica Civil Engineering*, 68(1), 1-7.

Pierott R, Hammad AWA, Haddad A, Garcia S, Falcon G (2021). A mathematical optimisation model for the design and detailing of reinforced concrete beams. *Engineering Structures*, 245, 112861.

Rao HS, Babu BR (2006) Optimized column design using genetic algorithm based neural networks. *Indian Journal of Engineering and Materials Sciences*, 13 (6), 503-511.

Rao RV, Savsani VJ, Vakharia DP (2011). Teaching–learning-based optimization: a novel method for constrained mechanical design optimization problems, *Computer-Aided Design*, 43(3), 303-315.

Rao RV (2016). Jaya: A simple and new optimization algorithm for solving constrained and unconstrained optimization problems. *International Journal of Industrial Engineering Computations*, 7(1), 19-34.

Sahab MG, Ashour AF, Toropov VV (2005). A hybrid genetic algorithm for reinforced concrete flat slab buildings. *Computers & Structures*, 83(8-9), 551-559.

Shooli AR, Vosoughi AR, Banan MR (2019). A mixed GA-PSO-based approach for performance-based design optimization of 2D reinforced concrete special moment-resisting frames. *Applied Soft Computing Journal*, 85, 105843.

Sönmez M (2011). Artificial Bee Colony algorithm for optimization of truss structures. *Applied Soft Computing*, 11(2), 2406-2418.

Tapao A, Cheerarot R (2017). Optimal parameters and performance of artificial bee colony algorithm for minimum cost design of reinforced concrete frames. *Engineering Structures*, 151, 802-820.

Temur R, Bekdaş G (2016). Teaching learning-based optimization for design of cantilever retaining walls. *Structural Engineering and Mechanics*, 57(4), 763-783.

Yousif ST, Najem RN (2013). Optimum cost design of reinforced concrete continuous beams using Genetic Algorithms. *International Journal of Applied Sciences and Engineering Research*, 2(1), 79-92.

Yücel M, Niğdeli SM, Bekdaş G (2023). Optimization of truss structures by using a hybrid population-based metaheuristic algorithm. *Arabian Journal for Science and Engineering*, 49, 5011-5026.

Challenge Journal of Concrete Research Letters

Research Article

Determining datum temperature and apparent activation energy: an approach for mineral admixtures incorporated cementitious systems

Muhammet Atasever [a,*], Mustafa Tokyay [b]

[a] Department of Civil Engineering, Abdullah Gül University, 38080 Kayseri, Türkiye
[b] Department of Civil Engineering, Middle East Technical University, 06800 Ankara, Türkiye

ABSTRACT

The maturity method is used to predict the strength of concrete by monitoring its temperature history. Accuracy of maturity method relies on the dependable determination of the datum temperature and the apparent activation energy. The current study introduces a new approach, complementing those in ASTM C1074-11, for determining the datum temperature and apparent activation energy. The experimental study involved using two different mineral additives to portland cement at 6%, 20%, and 35% replacement amounts. The mortars were then cured at temperatures of 5, 20, and 40 °C, and their strengths were determined. Subsequently, the datum temperatures and apparent activation energies for these mixtures were calculated using both the proposed approach and the alternatives from ASTM C1074-11. Strength estimations were conducted in conjunction with commonly used maturity functions. The results indicate that the proposed approach determines the datum temperature and apparent activation energy reliably for mineral admixture-incorporated mortars. Furthermore, the predicted strengths, derived from the datum temperature and apparent activation energy calculated through the proposed approach, show a closer alignment with the experimental results when applying the Nurse-Saul and Hansen-Pedersen equations, as opposed to the Rastrup and Weaver-Sadgrove models.

ARTICLE INFO

Article history:
Received 12 July 2024
Revised 31 August 2024
Accepted 12 September 2024

Keywords:
Maturity method
Datum temperature
Apparent activation energy
Mineral admixture

This is an open access article distributed under the CC BY licence.
© 2024 by the Authors.

1. Introduction

The maturity method is a technique that is used for estimating the strength of concrete by taking temperature and time into account. Accuracy of the method relies primarily on dependable determination of the datum temperature and apparent activation energy. Maturity of concrete is generally expressed in terms of a temperature-time relationship and its equivalent age. The most well-known function for the temperature-time relationship is the Nurse-Saul equation, as given in Eq. (1).

$$M = \sum_0^t (T - T_0) \cdot \Delta t \quad (1)$$

where M (degree-days or degree-hours) is maturity index at age t, T (°C) is the average concrete temperature during the time interval, Δt, T_0 (°C) is datum temperature and Δt (days or hours) is time interval.

The principal idea of Eq. (1) is that concretes of the same mix and maturity tend to exhibit same strength. However, due to its linear character, Nurse-Saul equation often fails to provide accurate strength estimates outside the temperature range of 0-40 °C (Miller et al. 2022; Soutsos et al. 2018, 2021). To address this limitation, several alternative equations have been proposed, including those by Rastrup (Rastrup 1954), Weaver and Sadgrove (Weaver and Sadgrove 1971), Hansen and Pedersen (Hansen and Pedersen 1977). These equations are given as Eq. (2) to Eq. (4), respectively.

$$t_e = \sum_0^t 2^{(T-T_r)/10} \cdot \Delta t \quad (2)$$

$$t_e = \sum_0^t \left(\frac{T+16}{T_r+16}\right)^2 \cdot \Delta t \quad (3)$$

$$t_e = \sum_0^t e^{\frac{-E_a}{R}\left(\frac{1}{T+273} - \frac{1}{T_r+273}\right)} \cdot \Delta t \quad (4)$$

* *Corresponding author.* Tel.: +90-352-224-8800 ; E-mail address: muhammet.atasever@agu.edu.tr (M. Atasever)
ISSN: 2548-0928 / DOI: https://doi.org/10.20528/cjcrl.2024.04.004

for $T \geq 20$ °C E_a=33500 J/mol
for $T < 20$ °C E_a=33500+1470 (20-T) J/mol

where t_e (days or hours) is equivalent age, E_a (J/mol) is apparent activation energy, R (8.314 J/mol-°K) is gas constant, T (°C) is the average concrete temperature during the time interval, Δt, T_r (°C) is reference temperature, Δt (days or hours) is time interval.

Among these four equations, the Nurse-Saul equation (Eq. (1)) requires a datum temperature, whereas the Hansen-Pedersen equation (Eq. (4)) necessitates an apparent activation energy. The datum temperature in here refers to the minimum temperature at which concrete begins to gain strength (Nixon et al. 2008) and the apparent activation energy is defined as the smallest amount of energy required for concrete to start gaining strength (Shukla and Mishra 2015). ASTM C1074-11 (2011) suggests that the datum temperature can be set at 0 °C and the apparent activation energy of 41.5 kJ/mol is recommended for the concrete made without mineral admixtures. The standard also provides three alternatives to determine the datum temperature and apparent activation energy of concrete. The primary difference between them lies in the assumed starting point for strength development. According to ASTM C1074-11 (2011), Alternative I (A1.1.7) considers it to begin at the final setting time, while Alternative II (A1.1.8.1) assumes it starts after the final setting time during the hydration acceleration period, provided that the concrete has a reasonable ultimate strength. Alternative III (A1.1.8.2) assumes that strength development begins immediately after mixing (Atasever 2017). Among these alternatives, the second one that is given by Eq. (5) is generally being used for concretes without mineral admixtures:

$$S = S_u \cdot \frac{k_T \cdot (t-t_0)}{1+k_T \cdot (t-t_0)} \qquad (5)$$

where, S (MPa) is compressive strength at age t, S_u (MPa) is ultimate strength, k_T (1/days) is rate constant, t_0 (days) is age at start of strength development.

The theory gained acceptance due to its hyperbolic character and being more related with the hydration characteristics of portland cement. The method suggests strength development commences once concrete fully sets (Knudsen 1984). Various researchers have commented that Eq. (5) may not be as effective for blended cements containing mineral admixtures (Atasever 2017; Elçi and Yılmaz 2009; Ferraro et al. 2016; Soutsos et al. 2018). The revision in ASTM C1074-19 (2019) further reinforces this perspective. This viewpoint stems from the observations that the hydration mechanism and kinetics of blended cements vary considerably throughout the process. The differences are basically related with the type, amount, and characteristics of the mineral admixtures in the cement. Mineral admixtures affect the hydration process both physically and chemically. Physical effects are dilution, dispersion, alteration of particle size distribution, and nucleation. Dilution effect generally retards hydration whereas the other effects usually accelerate it. Chemically, their influence is seen in pozzolanic reactions, latent hydraulic reactions, and other related processes (Lam et al. 2023; Lothenbach et al. 2011; Moula et al. 2023; Wang et al. 2018). Another limitation of the function is its tendency to overestimate the long-term strengths of samples due to the negative impact of high curing temperatures (Miller et al. 2022; Soutsos et al. 2017, 2018, 2021). In this context, number of variables come into scene: the dissolution and stability of components within the pore fluid, a high concentration of hydroxyl ions, and the resulting chemical reaction rates. These factors collectively influence both the amount of hydration products and the early-age strength development in blended cements containing mineral admixtures (Zhang et al. 2021; Zuo et al. 2019). Additionally, the behavior of cementitious systems with incorporated mineral admixtures during the early-stages can be clarified using the “through-solution process”. As highlighted by Tokyay (2016) and John and Lothenbach (2023), when the formation of hydration products primarily drives hydration, the water reaches saturation. This leads to uneven precipitation throughout its entire volume. Besides, in the later stages, adding mineral admixtures to portland cement leads to the formation of C-S-H gels through secondary hydration with portlandite. This process refines the pore structure and enhances the microstructure of the cementitious material. However, the distinct Ca/Si ratios in these cementitious systems cause differences in the interfacial transition zone (ITZ), affecting factors such as porosity, pore structure, and pore size. This variability also impacts the distribution of portland cement particles, which in turn influences the nucleation and precipitation of C-S-H gels (Dadsetan and Bai 2017; Liu et al. 2023; Lv et al. 2023).

This study describes a new methodology for determining the datum temperature and the apparent activation energy in cementitious systems with mineral admixtures. Employing a hyperbolic framework as explicated in Eq. (5), the proposed approach computes the ultimate strength and rate constant by considering early-age strength data recorded up to 14 days. This may seem as a contradiction for trass and blast furnace slag incorporated cementitious systems since pozzolanic and latent hydraulic reactions are generally far more gradual than hydration reactions. However, taking the early age data makes it possible to predict the time when a critical (sufficient) amount of calcium hydroxide is produced upon hydration of the portland cement and thus pozzolanic or latent hydraulic reactions start to contribute to the strength. So, Eq. (5) is rewritten as:

$$S = S_u \cdot \frac{k_T \cdot (t-t_{cr})}{1+k_T \cdot (t-t_{cr})} \qquad (6)$$

where, S (MPa) is compressive strength at age t, S_u (MPa) is ultimate strength, k_T (1/days) is rate constant, t_{cr} (days) is the age when the mineral admixture starts to contribute the strength.

The difference between Eqs. (5) and (6) lies in the use of t_{cr} instead of t_0. The calculation of t_{cr} involves two stages. In the first stage, the ultimate strength and rate constant are calculated. These two parameters, computed for each curing temperature, were derived using the test ages of 2, 7, and 14 days along with the corresponding strengths. However, a constraint was applied during the calculation of ultimate strength: the calculated ultimate strength must exceed the measured strength at 90 days. If not, the 90-day strength is taken as the ultimate strength. In the second stage, a strength-age graph is plotted for each curing temperature to determine t_{cr}, where a line is fitted. The age corresponding to half of the ultimate strength on this line is defined as the age when the mineral admixture starts to contribute to the strength. The datum temperatures and apparent activation energies for trass- and blast furnace slag-incorporated mortar mixes using the proposed approach and the methods given in ASTM C1074-11 (2011). Subsequently, the strength of these mixtures is evaluated via the Nurse-Saul, Rastrup, Weaver and Sadgrove, and Hansen and Pedersen equations. Comparative analysis is then conducted between the strength values derived from each equation.

2. Materials and Method

A portland cement (CEM I 42.5 R) was combined with two mineral admixtures: a volcanic tuff, trass (TRS) and a ground granulated blast furnace slag (BFS). These were used at replacement levels of 6%, 20%, and 35% by mass, with the specified levels determined in accordance with the guidelines outlined in TS EN 196-1 (2016). Standard sand was used in all mortar mixtures. Table 1 details the chemical and physical properties of the materials utilized in the study.

Table 1. Chemical and physical properties of the materials used.

Properties (%)	PC cement*	TRS	BFS
SiO_2	18.6	69.7	43.0
Al_2O_3	4.9	12.0	11.3
Fe_2O_3	2.5	1.7	0.9
CaO	61.6	2.8	33.0
MgO	2.3	0.9	6.2
SO_3	3.3	0.1	1.2
Na_2O	0.3	1.1	0.3
K_2O	0.8	1.8	0.7
TiO_2	-	0.3	0.6
LOI	5.1	7.3	0.3
Blaine fineness (m^2/kg)	340	540	470
Density (g/cm^3)	3.0	2.3	2.9

* The XRF result for PC cement was previously reported in the study of Atasever and Tokyay (2018).

The mixing, compaction, and moulding of mixtures were performed in accordance with TS EN 196-1 (2016), while maintaining a constant flow value (110±5%) as stipulated by ASTM C1437-20 (2020). All mortar samples were cast in moulds of 40×40×160 mm dimensions. Subsequently, the specimens were subjected to curing temperatures of 5, 20, and 40 °C until the designated test ages of 2, 7, 14, 28, and 90 days. The selection of test ages is based on the incorporation of mineral admixtures in the study. According to the proposed approach presented in Eq. (6), the ultimate strength must exceed the 90-day strength, consistent with the hydration mechanism of cementitious systems. The 2-day test was chosen based on the assumption that strength development in blends containing mineral admixtures does not begin before 2 days, as indicated in Eq. (6). On the other hand, the curing temperatures were chosen to encapsulate the spectrum of environmental conditions that concrete is likely to encounter across various regions of Türkiye, as documented in the study (Dombaycı 2009). Although regional temperature variations exist, the selected temperatures are representative of the thermal fluctuations experienced on a national scale, thereby facilitating a thorough evaluation of concrete performance under realistic and applicable conditions. The compressive strength obtained are the average of six specimens. The mixture proportions of the mortars are given in Table 2.

Table 2. Proportions of mortar mixtures (wt. %).

Mixture ID	PC cement	TRS	BFS	(w/b)
PC Control**	100	-	-	0.56
PC-TRS6	94	6	-	0.59
PC-TRS20	80	20	-	0.67
PC-TRS35	65	35	-	0.71
PC-BFS6	94	-	6	0.56
PC-BFS20	80	-	20	0.56
PC-BFS35	65	-	35	0.56

** The mix proportion for PC Control was previously employed in the study of Atasever and Tokyay (2018).

The normal consistency of pastes-having the same mixture proportions as specified in Table 2-was first determined according to ASTM C187-16 (2016). Subsequently, the final setting time of these mixtures was ascertained using ASTM C191-21 (2021). The results are presented in Fig. 1.

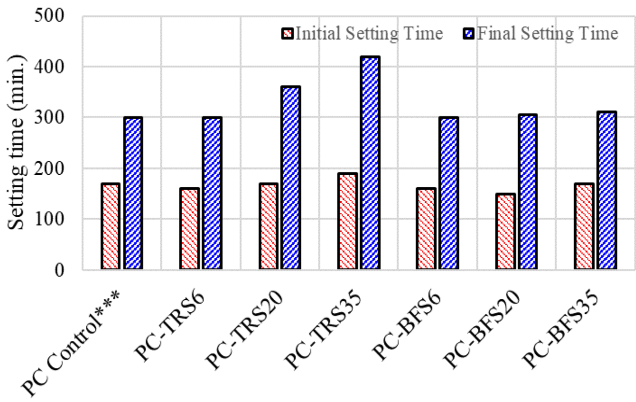

*** The setting time results for PC Control was previously reported in the study of Atasever and Tokyay (2018).

Fig. 1. Results of setting time of mixtures.

3. Results and Discussion

The strength development curves for all mixes cured at 5, 20 and 40 °C was plotted in Fig. 2 after 2, 7, 14, 28 and 90 days of curing.

The relationships between PC Control and the strength of mortar with mineral admixture over time (measured in days) show a striking similarity for the first 28 days. However, beyond 28 days, a notable difference emerges in the PC Control, PC-TRS20, and PC-BS6 mixtures. Mixtures cured at 20 °C displayed a reduced strength in comparison to those cured at 40 °C, indicating a temperature-dependent variation in the strength development of the mortar mixtures with mineral admixtures. This might be related to crossover effect, where high curing temperatures accelerate hydration and cause uneven distribution of hydration products, resulting in reduced porosity and higher early-age strength, but increased porosity and diminished strength at later ages (Escalante-García and Sharp 2001; Kim et al. 2002; Soutsos and Kanavaris 2020).

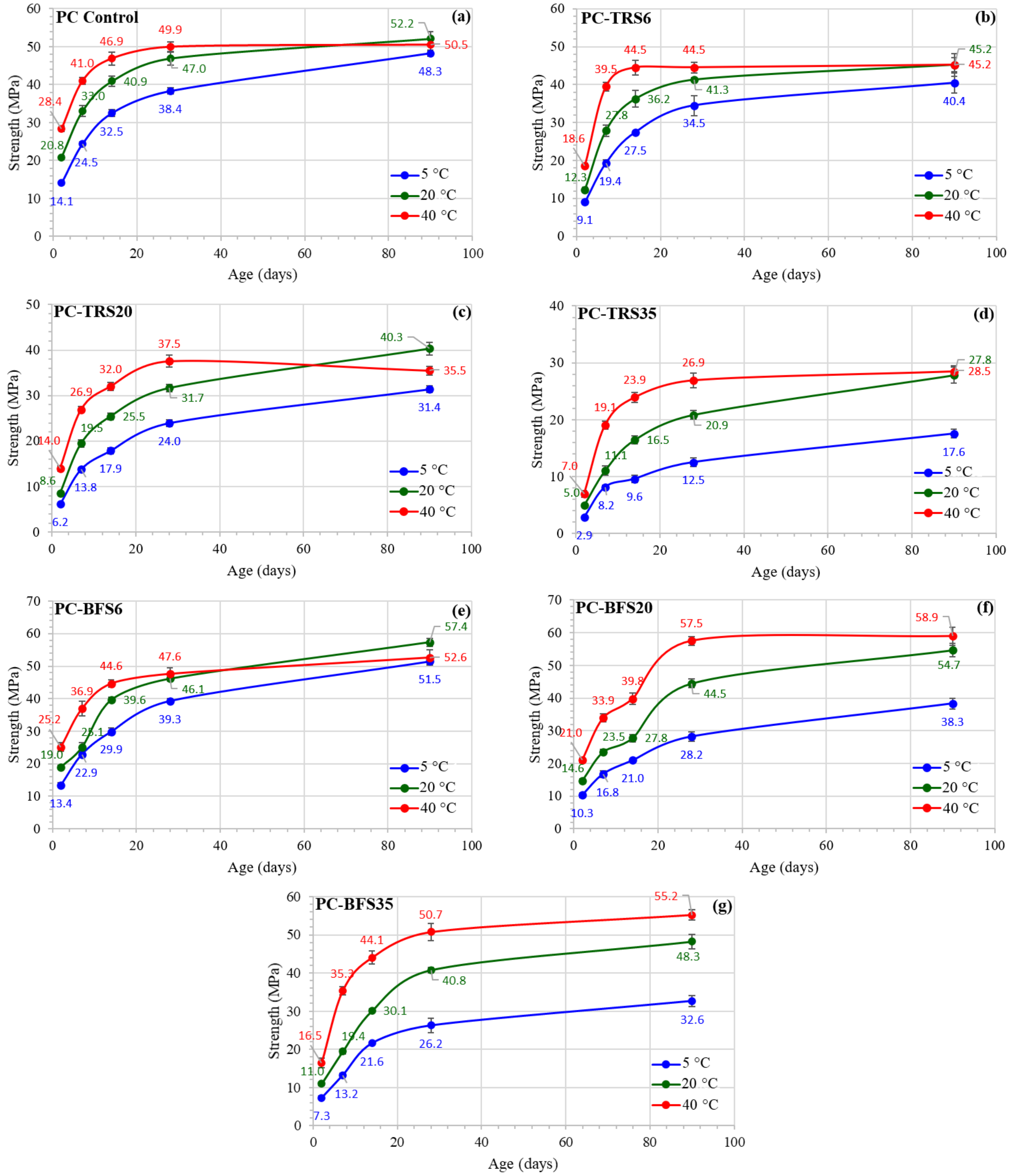

Fig. 2. Strength development curves at different curing temperature for:
(a) PC Control; (b) PC-TRS6; (c) PC-TRS20; (d) PC-TRS35; (e) PC-BFS6; (f) PC-BFS20; (g) PC-BFS35.

In low-heat concretes, strength development is slower, complicating late-age strength predictions. Adjusting the thermal curing parameters, such as heating rate, peak temperature, and curing duration, becomes crucial in addressing this challenge. Properly considering the crossover effect ensures accurate strength prediction and may necessitate modifications to the maturity equation to achieve precise forecasting of compressive strength (Klausen et al. 2018; Wang et al. 2023). Conversely, in the case of PC-TRS6 and PC-TRS35, the 90-day strengths exhibit minimal difference between samples cured at 20 and 40 °C. The observed consistency in 90-day strength at both 20 and 40 °C curing temperatures can be attributed to the eventual completion of hydration reactions that initially progress at a slower rate. This gradual completion may counterbalance the reduced speed of chemical reactions at room temperatures, leading to similar strengths across both temperature conditions.

3.1. Determining datum temperature and apparent activation energy: ASTM C1074-11 methods and the proposed approach

Three alternatives, detailed in ASTM C1074-11 (2011), along with proposed approach, were employed to determine apparent activation energy and datum temperature based on the strength data. Alternative 1 stands out among the three options in ASTM C1074-11 (2011), as it designates the final setting time as the age to begin strength development in cementitious materials. In contrast, other two alternatives predominantly utilize compressive strength results. Notably, Alternative 3 assumes that strength development in cementitious materials starts at the moment the cement-water reaction begins. Alternative 2, leveraging a hyperbolic equation, proves particularly pertinent for cements without mineral additives, unveiling a correlation absent in other variants. Therefore, a novel approach has been proposed, aiming to harmonize these discrepancies. This approach refines Eq. (5), ensuring that the ultimate strength reliably exceeds the 90-day benchmark. It further identifies the age to that the mineral admixture starts to contribute the strength by pozzolanic or latent hydraulic reactions. After completing the determination of rate constants and ultimate strengths by both ASTM C1074-11 (2011) procedures and the proposed approach, datum temperatures and apparent activation energies were computed, and results are given in Table 3. The activation energies, calculated from strengths, showed variations according to ASTM C1074-11 (2011) methods, ranging between 3.9 and 45.4 kJ/mol. In contrast, in the proposed approach, these values ranged from 20.5 to 33.8 kJ/mol. In the proposed approach, it was observed that as the amount of mineral additive increased, regardless of the type of mineral additive, the apparent activation energies of the blends increased compared to the PC Control. The only exception to this situation belongs to the PC-TRS6. Trass, which was 6 % by weight in this mixture, may have caused the dispersion of cement particles, allowing more space for the hydration of portland cement. This phenomenon has been observed in numerous studies involving the use of small quantities of mineral additives (Wang et al. 2024; Zhang et al. 2023; Jiang et al. 2023).

Table 3. Datum temperature and apparent activation energy of cementitious systems, calculated using different alternatives.

Mixture ID	Datum temperature (°C)			
	ASTM C1074-11 (2011)			Proposed approach
	Alternative 1	Alternative 2	Alternative 3	
PC Control****	-15.9	-7.0	1.6	-10.9
PC-TRS6	-26.6	-15.9	4.9	-9.2
PC-TRS20	-24.6	-7.5	4.1	-4.6
PC-TRS35	-104.9	-3.9	-0.5	1.2
PC-BFS6	-24.8	-6.9	-27.8	-9.0
PC-BFS20	-154.7	-10.2	-0.5	-9.6
PC-BFS35	-122.7	-1.4	-0.1	-7.2
	Apparent activation energy (kJ/mol)			
PC Control*****	19.3	24.7	37.9	22.5
PC-TRS6	14.4	21.2	45.3	20.5
PC-TRS20	15.2	34.2	39.7	29.6
PC-TRS35	5.8	34.2	31.0	33.8
PC-BFS6	15.8	26.6	15.5	22.7
PC-BFS20	3.9	23.6	26.1	23.6
PC-BFS35	5.0	26.9	32.7	25.3

**** The datum temperatures and apparent activation energies for PC Control, calculated according to the methods specified in ASTM C1074-11 (2011), were previously reported in the study of Atasever and Tokyay (2018).

The datum temperature for each mixture was determined through three different methods, as detailed in ASTM C1074-11 (2011) and the proposed approach. The differences in datum temperatures are primarily attributed to the differing approaches of each method in considering the time to begin strength development in the mixtures. In the case of the PC Control, datum temperatures exhibit relative consistency across these alternatives. Conversely, mixtures containing mineral additives show a tendency to produce illogical datum temperature results, especially with Alternative 1, as the amount of mineral additives increases. While the datum temperatures for each mixture, calculated using Alternatives 2 and 3, range from -27.8 to 4.9 °C, the range for the proposed approach varies between -11.2 and 1.2 °C. Although ASTM C1074-11 (2011) recommends a datum temperature of 0 °C for Type I cement without mineral admixtures, there is no universally applicable datum temperature for blends containing minerals as reported in the literature.

3.2. Assessment of the proposed approach

The maturities of the seven distinct mixtures were determined employing the equations given by Nurse-Saul (Eq. (1)), Rastrup (Eq. (2)), Weaver and Sadgrove (Eq. (3)), Hansen, and Pedersen (Eq. (4)). The datum temperature and apparent activation energy parameters utilized in these equations were derived by the proposed approach. Assuming a logarithmic relationship between the maturity index and strength for each equation, the compressive strengths at 2, 7, 14, 28, and 90 days for each mixture cured at 5, 20, and 40 °C were estimated. These theoretical values were then compared with the corresponding experimental results obtained. The comparative analysis is illustrated in Fig. 3.

In the context of these methodologies, the Nurse-Saul mandates the incorporation of datum temperature, whereas the Hansen-Pedersen is predicated upon the requisite of an apparent activation energy. In contrast, the Rastrup and Weaver-Sadgrove methods function exclusively based on the temperature history of the blends. Empirical analysis has demonstrated that, in terms of accuracy in strength predictions, the Nurse-Saul and Hansen-Pedersen equations outperform those of Rastrup and Weaver-Sadgrove, maintaining a margin of error confined to within 10 %. The observed discrepancy can be ascribed to the underlying assumptions of the Nurse-Saul equation, which asserts a linear correlation between strength development and temperature. Conversely, the Hansen-Pedersen function hypothesizes an exponential increase in strength gain rate with temperature (Soutsos et al. 2021). The linear model of the Nurse-Saul equation often results in an overestimation of the effects of lower early-age curing temperatures on the strength. In contrast, the exponential model of the Hansen-Pedersen function tends to underestimate the strength of blends in the early ages. Additionally, the Rastrup function proposes that the rate of reaction doubles with a 10 °C increment in reaction temperature, a principle that is paralleled in the Weaver-Sadgrove equation (Soutsos et al. 2018; Kanavaris et al. 2023). Nevertheless, such exponential strength gain rates are not commonly observed in trass and blast furnace slag incorporated blends, leading to deviations in strength estimates exceeding the 10 % margin of error.

4. Conclusions

This study investigated the determination of datum temperature and apparent activation energy values in trass and slag incorporated mortars, comparing traditional methods with a new approach. Furthermore, the datum temperatures and apparent activation energies determined through the proposed approach were employed in the maturity approaches of Nurse-Saul, Rastrup, Weaver-Sadgrove, and Hansen-Pedersen to estimate strength under various curing conditions and ages. Subsequently, these estimated strength values were compared with the experimental strength results. The following conclusions can be drawn:

- Excluding PC-TRS20, and PC-BFS6, the observed strength indicates a general trend where higher curing temperatures are associated with an increase in strength, while lower curing temperatures correspond to a decrease in strength.
- Datum temperature values, calculated using the proposed approach, range from -11 to 1 °C, while apparent activation energy values range between 20.5 kJ/mol and 33.8 kJ/mol. An observed trend indicates that as the mineral contribution increases in the cementitious system, the apparent activation energy value also increases.
- The strength estimation results, based on data temperatures and apparent activation energies derived through the proposed approach, indicated that the Nurse-Saul and Hansen-Pedersen equations provide predicted strengths much closer to the experimental results than the Rastrup and Weaver-Sadgrove models for the mineral admixture-incorporated mortars.
- The approach proposed in this investigation resulted in a reasonable determination of datum temperatures and apparent activation energies for trass- and slag-incorporated cement mortars.
- Similar research with other types of mineral admixtures would further refine the approach.

Acknowledgements

None declared.

Funding

The authors received no financial support for the research, authorship, and/or publication of this manuscript.

Conflict of Interest

The authors declared no potential conflicts of interest with respect to the research, authorship, and/or publication of this manuscript.

Author Contributions

All of the authors made substantial contributions to conception and design, or acquisition of data, or analysis and interpretation of data; were involved in drafting the manuscript or revising it critically for important intellectual content; and gave final approval of the version to be published.

Data Availability

The datasets created and/or analyzed during the current study are not publicly available, but are available from the corresponding author upon reasonable request.

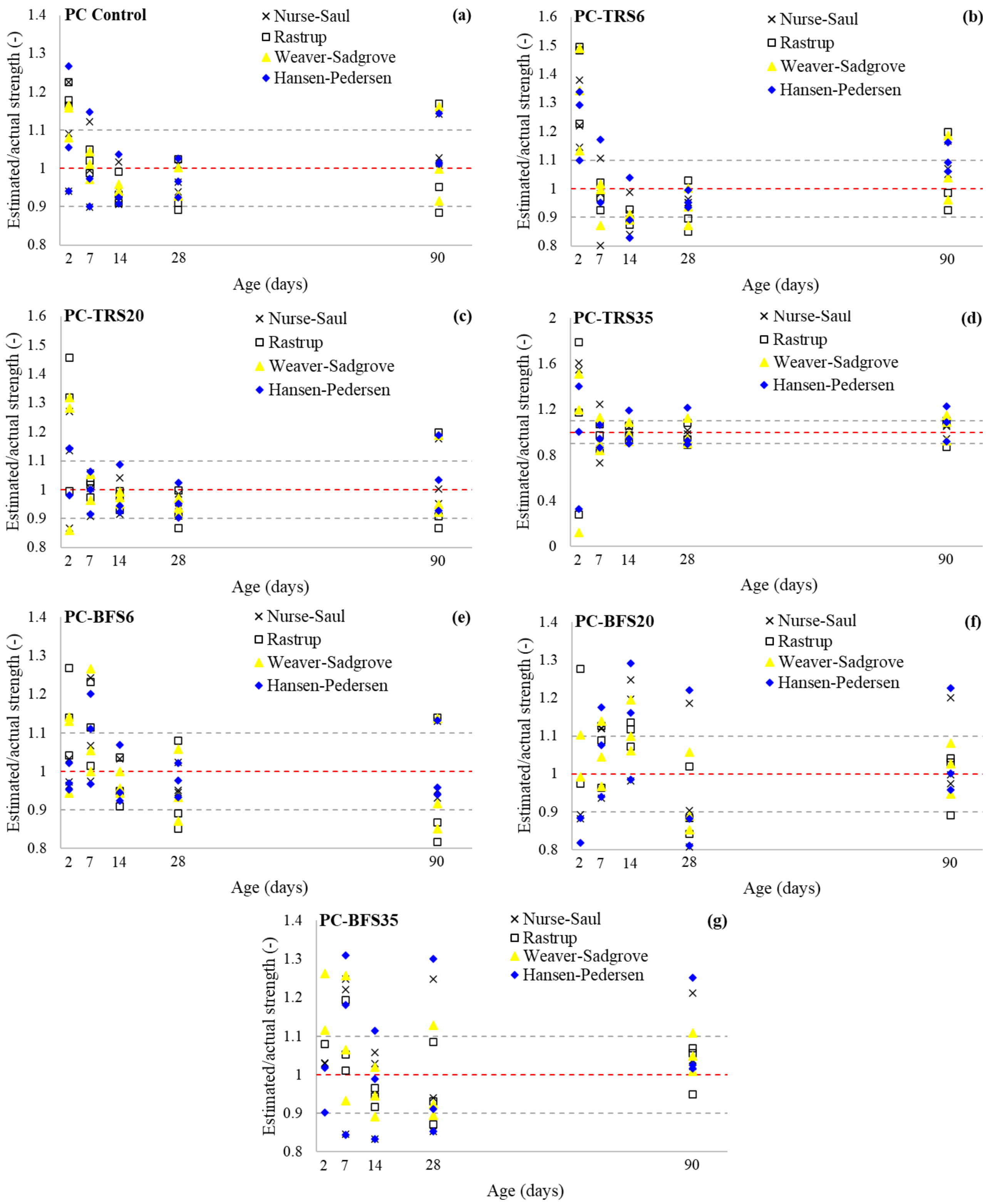

Fig. 3. Ratio of estimated/actual strengths for:
(a) PC Control; (b) PC-TRS6; (c) PC-TRS20; (d) PC-TRS35; (e) PC-BFS6; (f) PC-BFS20; (g) PC-BFS35.

References

ASTM C1074-11. (2011) Standard Practice for Estimating Concrete Strength by the Maturity Method. American Society for Testing and Materials, West Conshohocken, PA.

ASTM C1074-19. (2019) Standard Practice for Estimating Concrete Strength by the Maturity Method. American Society for Testing and Materials, West Conshohocken, PA.

ASTM C1437-20. (2020) Standard Test Method for Flow of Hydraulic Cement Mortar. American Society for Testing and Materials, West Conshohocken, PA.

ASTM C187-16. (2016) Standard Test Method for Amount of Water Required for Normal Consistency of Hydraulic Cement Paste. American Society for Testing and Materials, West Conshohocken, PA.

ASTM C191-21. (2021) Standard Test Methods for Time of Setting of Hydraulic Cement by Vicat Needle. American Society for Testing and Materials, West Conshohocken, PA.

Atasever M (2017). Maturity and Equivalent Age Functions of Mineral Admixtures Incorporated Mortars. *M.Sc. thesis*, Middle East Technical University, Ankara, Türkiye.

Atasever M, Tokyay M (2018). Comparison of three alternatives for determining datum temperature and activation energy to estimate concrete strength by maturity method. *13th International Congress on Advances in Civil Engineering*, İzmir, Türkiye, 87-88.

Dadsetan S, Bai J (2017). Mechanical and microstructural properties of self-compacting concrete blended with metakaolin, ground granulated blast-furnace slag and fly ash. *Construction and Building Materials*, 146, 658–667.

Dombaycı ÖA (2009). Degree-days maps of Turkey for various base temperatures. *Energy*, 34(11), 1807-1812.

Elçi H, Yılmaz A (2009). Mineral katkılı çimentolarla üretilen betonun dayanımını tahmin etmede olgunluk yönteminin kullanılması. *Journal of the Faculty of Engineering and Architecture of Gazi University*, 24(3), 549–558. (in Turkish)

Escalante-García JI, Sharp JH (2001). The microstructure and mechanical properties of blended cements hydrated at various temperatures. *Cement and Concrete Research*, 31(5), 695–702.

Ferraro CC, Paris JM, Townsend TG, Tia M (2016). Evaluation of alternative pozzolanic materials for partial replacement of portland cement in concrete, Florida Department of Transportation Research Project, Gainesville, FL, USA. https://rosap.ntl.bts.gov/view/dot/31986 [accessed 09-05-2024].

Hansen PF, Pedersen EJ (1977). Maturity computer for controlled curing and hardening of concrete. *Nordisk Betong*, 21–25.

Jiang J, Wang, F, Wang L, Zhang J, Wang L (2023). Experimental investigation on effects of polyaniline-modified-lignin on cement-based materials: Strength, hydration and dispersion. *Construction and Building Materials*, 394, 131853.

John E, Lothenbach B (2023). Cement hydration mechanisms through time – a review. *Journal of Materials Science*, 58(24), 9805-9833.

Kanavaris F, Soutsos M, Chen JF (2023). Enabling sustainable rapid construction with high volume GGBS concrete through elevated temperature curing and maturity testing. *Journal of Building Engineering*, 63, 105434.

Kim JK, Han SH, Song YC (2002). Effect of temperature and aging on the mechanical properties of concrete: Part I. Experimental results. *Cement and Concrete Research,* 32, 1087-1094.

Klausen AE, Kanstad T, Bjøntegaard Ø, Sellevold EJ (2018). The effect of realistic curing temperature on the strength and E-modulus of concrete. *Materials and Structures,* 51(6), 168.

Knudsen T (1984). The dispersion model for hydration of portland cement I. General concepts. *Cement and Concrete Research*, 14(5), 622–630.

Lam A, Hamzaoui R, Kindinis A (2023). Structural and mechanical studies of a ground-granulated blast-furnace slag (GGBS) based binder and its use in earth concrete. *Materials Today: Proceedings*, in press.

Liu W, Zhu H, Wu X, Wan Y, Zheng W, Li H (2023). Comparative study on the performance of ultra-fine fly ash prepared by different techniques in Portland cement and alkali-activated material. *Construction and Building Materials*, 397, 132362.

Lothenbach B, Scrivener K, Hooton RD (2011). Supplementary cementitious materials. *Cement and Concrete Research*, 41(12), 1244–1256.

Lv X, Shi Y, Wang Y, Li J (2023). Utilization of phosphorus slag as fly ash replacement in low-heat Portland cement blends: Comparative study of hydration behaviors, physical properties, and life-cycle assessment. *Construction and Building Materials*, 396, 132346.

Miller D, Ho NM, Talebian N (2022). Monitoring of in-place strength in concrete structures using maturity method – An overview. *Structures*, 44, 1081–1104.

Moula S, Fraj AB, Wattez T, Bouasker M, Ali NBH (2023). Mechanical properties, carbon footprint and cost of ultra-high performance concrete containing ground granulated blast furnace slag. *Journal of Building Engineering*, 79, 107796.

Nixon JM, Schindler AK, Barnes RW, Wade SA (2008). Evaluation of the maturity method to estimate concrete strength in field applications, Research report no. 2. Alabama Department of Transportation, ALDOT research project 930-950. https://eng.auburn.edu/files/centers/hrc/930-590-2.pdf [accessed 09-05-2024].

Rastrup E (1954). Heat of hydration in concrete. *Magazine of Concrete Research,* 6(17), 79–92.

Shukla MK, Mishra SP (2015). In place strength of cement mortar/concrete using maturity and activation energy. *International Journal of Advanced Engineering Research and Studies*, 79–82.

Soutsos M, Hatzitheodorou A, Kanavaris F, Kwasny J (2017). Effect of temperature on the strength development of mortar mixes with GGBS and fly ash. *Magazine of Concrete Research*, 69(15), 787–801.

Soutsos M, Kanavaris F (2020). Compressive strength estimates for adiabatically cured concretes with the Modified Nurse-Saul (MNS) maturity function. *Construction and Building Materials*, 255, 119236.

Soutsos M, Kanavaris F, Elsageer M (2021). Accuracy of maturity functions' strength estimates for fly ash concretes cured at elevated temperatures. *Construction and Building Materials*, 266, 121043.

Soutsos M, Kanavaris F, Hatzitheodorou A (2018). Critical analysis of strength estimates from maturity functions. *Case Studies in Construction Materials*, 9, e00183.

Tokyay M (2016). Cement and Concrete Mineral Admixtures. 1st ed. CRC Press, Taylor and Francis Group, Florida, USA.

TS EN 196-1 (2016). Methods of testing cement-Part 1: Determination of strength. Turkish Standards Institute, TSE, Ankara, Türkiye.

Wang D, Shi C, Farzadnia N, Shi Z, Jia H, Ou Z (2018). A review on use of limestone powder in cement-based materials: Mechanism, hydration and microstructures. *Construction and Building Materials*, 181, 659–672.

Wang L, Wang J, Wang H, Qian X, Fang Y, Ge Y, Wang X, Zhao X, Amaral MLD (2024). Ascorbic acid: A green admixture for eco-efficient metakaolin blended cement with enhanced properties and corrosion resistance. *Cement and Concrete Composites*, 146, 105405.

Wang L, Zhou H, Zhang J, Wang Z, Zhang L, Nehdi ML (2023). Prediction of concrete strength considering thermal damage using a modified strength-maturity model. *Construction and Building Materials*, 400, 132779.

Weaver J, Sadgrove BM (1971). Striking Times of Formwork-Tables of Curing Periods to Achieve Given Strength. Construction Industry and Information Association, London, England.

Zhang J, Pan G, Yan Y (2021). Early hydration, mechanical strength and drying shrinkage of low-carbon alkali-activated Ti-extracted residues-fly ash cement and mortars. *Construction and Building Materials*, 293, 123517.

Zhang M, Li H, Na M, Zhou B, Zhang J (2023). Improving dispersion of recycled GFRP fiber in cement mortar with sodium hexametaphosphate. *Cement and Concrete Composites,* 143, 105232.

Zuo Y, Nedeljković M, Ye G (2019). Pore solution composition of alkali-activated slag/fly ash pastes. *Cement and Concrete Research,* 115, 230–250.